Zonostrophic instability

Kaushik Srinivasan * and W. R. Young

Scripps Institution of Oceanography, University of California at San Diego

ABSTRACT

Zonostrophic instability leads to the spontaneous emergence of zonal jets on a β-plane from a jetless basic-state flow which is damped by bottom drag and driven by a random body force. Decomposing the barotropic vorticity equation into the zonal-mean and eddy equations, and neglecting the eddy-eddy interactions, defines the quasi-linear (QL) system. Numerical solution of the QL system shows zonal jets with length scales comparable to jets obtained by solving the nonlinear (NL) system.

Starting with the QL system, one can construct a deterministic equation for the evolution of the two-point single-time correlation function of the vorticity, from which one can obtain the Reynolds stress that drives the zonal mean flow. This deterministic system has an exact nonlinear solution, which is an isotropic and homogenous eddy field with no jets. We characterize the linear stability of this jetless solution by calculating the critical stability curve in the parameter space and successfully comparing this analytic result with numerical solutions of the QL system. But the critical drag required for the onset of NL zonostrophic instability is sometimes a factor of six smaller than that for QL zonostrophic instability.

Near the critical stability curve, the jet scale predicted by linear stability theory agrees with that obtained via QL numerics. But on reducing the drag, the emerging QL jets agree with the linear stability prediction at only short times. Subsequently jets merge with their neighbors till the flow matures into a state with jets which are significantly broader than the linear prediction, but have have similar spacing as NL jets.

1. Introduction

Zonal flows are banded, anisotropic, weakly fluctuating alternating jets that form spontaneously and persist indefinitely in an otherwise turbulent plasma or planetary fluid (Diamond et al. 2005; Vasada and Showman 2005). The subject started with Rhines' 1975 discovery that freely evolving barotropic β-plane turbulence transfers energy into zonal shear modes with zero frequency (Rhines 1975). We follow Galperin et al. (2006) in referring to the development and persistence of these anisotropic planetary flows as "zonation". Williams (1978) showed that zonation occurs in statistically steady forced-dissipative flows on the sphere, and proposed this as an explanation of the banded structure of the planetary circulations of Jupiter and Saturn.

Figure 1 shows a typical example of fully developed zonation obtained by numerical solution of the barotropic β-plane potential vorticity equation:

$$\zeta_t + u\zeta_x + v\zeta_y + \beta v = \xi - \mu\zeta + \nu_n \nabla^{2n}\zeta\,. \qquad (1)$$

A streamfunction $\psi(x, y, t)$ is used to obtain the incompressible velocity $(u, v) = (-\psi_y, \psi_x)$, with relative vorticity $\zeta = \psi_{xx} + \psi_{yy}$. The flow is energized by the forcing ξ, and is damped by a combination of Ekman drag μ and hyperviscosity ν_n (with $n = 4$ in our numerical simulations). The main features of the statistically steady flow in Figure 1, such as the sharp eastward jets, the broader westward return flows, and the sawtooth relative vorticity, are familiar from many earlier studies of statistically steady, stochastically forced, dissipative β-plane turbulence in doubly periodic geometry (Danilov and Gurarie 2004; Danilov and Gryanik 2004; Maltrud and Vallis 1991; Vallis and Maltrud 1993), and on the sphere (Williams 1978; Nozawa and Yoden 1997; Huang and Robinson 1998; Scott and Polvani 2007).

The forcing $\xi(x, y, t)$ on the right of (1) is a rapidly decorrelating, isotropic, spatially homogeneous, random process that injects energy and enstrophy into a narrow band of wavenumbers centered on a "forced wavenumber" k_f (see Appendix A for details of the implementation). Following Lilly (1969) and Williams (1978), exogenous stochastic forcing, modeling small-scale convection or baroclinic activity, is now a standard protocol used in barotropic and shallow-water studies of forced-dissipative zonation. The spacing of the jets in Figure 1 is significantly greater than the typical length scale of the forcing, k_f^{-1}, which is an indication of either the inverse cascade, or of a spectrally nonlocal transfer of energy (Huang and Robinson 1998).

A striking feature of β-plane zonation is that the translational symmetry, $y \to y + a$, of the equation of motion

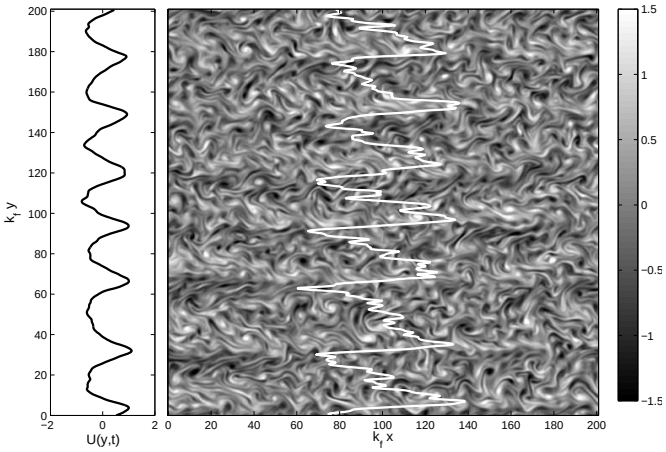

FIG. 1. *Nonlinear (NL) zonal jets.* Left panel: a snapshot of the zonally averaged velocity $U(y,t)$ obtained from a solution of (1) in a doubly periodic domain $2\pi L \times 2\pi L$ with $k_f L = 32$, where k_f is the dominant wavenumber of the forcing ξ. Right panel: a snapshot of the vorticity ζ, with overlaid zonally averaged vorticity $-U_y(y,t)$ (solid white curve). The parameter values for this run are $\mu_* = 0.01824$ and $\beta_* = 1.0$. The snapshot is at $2\mu t = 25$ with spin-up from rest.

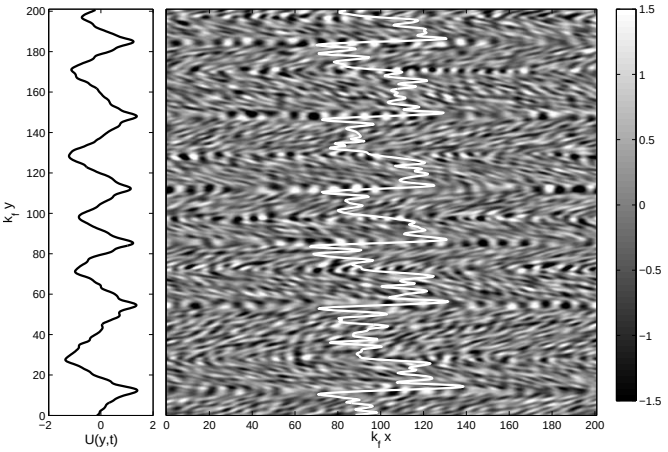

FIG. 2. *Quasilinear (QL) zonal jets.* Left panel: a snapshot of the zonally averaged velocity $U(y,t)$ obtained by integrating the QL system (3), (4) and (6). Right panel: a snapshot of the QL vorticity ζ, with overlaid zonally averaged vorticity $-U_y$ (solid white curve). The parameters for this run are the same as the nonlinear solution in Figure 1 i.e., $\mu_* = 0.0182$, $\beta_* = 1$ and $k_f L = 32$. The snapshot is at $2\mu t = 40$ after spin-up from rest.

(1) is spontaneously broken: the locations of the eastward maxima in Figure 1 are an accident of the initial conditions and of the random number generator used to create ξ. But after the jets form, they remain in the same position, apparently forever. Once these robust quasi-steady jets are in place, their dynamics can be discussed in mechanistic terms using concepts such as potential vorticity mixing, the resilience of transport barriers at the velocity maxima, radiation stress and shear-straining of turbulent eddies. But the primary question addressed here is why the jets form in the first place, given that the forcing ξ does not select particular locations. Following earlier investigations of this phenomenon (Farrell and Ioannou 2007; Manfroi and Young 1999), we show that zonation can be understood as symmetry-breaking instability of an isotropic, spatially homogeneous and jetless β-plane flow .

In section 2 we introduce the eddy-mean decomposition and discuss a statistical method, previously used by Farrell and Ioannou (1993b, 2003, 2007), Marston et al. (2008), and Tobias et al. (2011), which is the basis of our linear stability analysis of zonostrophic instability. This method amounts to forming quadratic averages of the equations of motion and then discarding third-order cumulants. Farrell and Ioannou (2003, 2007) refer to this method as stochastic structural stability theory (SSST), while Marston et al. (2008) call it the second-order cumulant expansion, or CE2. SSST and CE2 are completely equivalent, and only one name is required. We have therefore adopted the more descriptive CE2 terminology of Marston et al. (2008).

In section 3 we present a physical space re-formulation of CE2 which has analytic advantages over earlier numerically oriented formulations. Within the context of CE2, section 4 provides a complete analytic description of zonostrophic instability obtained by linearizing around an exact isotropic and homogeneous solution with no jets. As in Farrell and Ioannou (2007), zonation is understood as a linear instability of CE2: part of the linearly unstable eigenmode is a zonal flow. This linear stability problem is characterized by two control parameters, a non-dimensional drag parameter μ_* and a non-dimensional planetary parameter β_*, and we determine the CE2 zonostrophic stability boundary in the (β_*, μ_*)-parameter plane. An important property of CE2 zonostrophic instability is that the most unstable wavenumber, which determines the meridional scale of the exponentially growing jets, is well away from zero. Because the instability unfolds around a nonzero wavenumber, CE2 zonostrophic instability is not properly a negative-viscosity instability. This point is reinforced in section 5 by showing that the CE2 eddy viscosity is identically zero. Section 6 is a comparison between the analytic results and direct numerical simulations of the nonlinear system. Section 7 is the discussion and conclusion. The more technical aspects of the paper are in five appendices.

2. The eddy-mean decomposition and quasilinear (QL) dynamics

We use an eddy-mean decomposition

$$\psi(x,y,t) = \bar{\psi}(y,t) + \psi'(x,y,t)\,, \tag{2}$$

where the overbar denotes a zonal average; we also denote the zonal mean velocity as $U(y,t) = \bar{u}(y,t)$. Applying this average to (1) results in the zonal mean momentum equation

$$\partial_t U + \partial_y \left(\overline{u'v'}\right) = -\mu U + \nu \partial_y^2 U\,, \tag{3}$$

and the eddy vorticity equation

$$\zeta'_t + U\zeta'_x + (\beta - U_{yy})\psi'_x + \mathrm{EENL} = \xi - \mu\zeta' + \nu\nabla^2\zeta'\,. \tag{4}$$

In (4), the eddy-eddy nonlinearity is

$$\mathrm{EENL} \stackrel{\mathrm{def}}{=} \psi'_x\zeta'_y - \psi'_y\zeta'_x - \left(\overline{\psi'_x\zeta'}\right)_y\,. \tag{5}$$

In addition to the zonal average, the overbar includes a running time average over a short interval so that $\bar{\xi}(y,t)$ does not appear on the right of (3). In presenting equations subsequently used to obtain analytic results we use $n = 1$ for the viscosity.

Quasilinear (QL) dynamics

The main results in this paper are obtained with a quasilinear (QL) system, which is defined by taking

$$\mathrm{EENL} \to 0 \tag{6}$$

in (4). Figure 2 shows a QL solution at the same parameter values as the fully nonlinear (NL) solution as Figure 1. Because of the coupling between the mean and the eddies, the QL system is nonlinear, and Figure 2 shows that QL dynamics still results in the spontaneous formation of quasisteady zonal jets.

Comparing the left panels in Figures 1 and 2, one sees that the QL jets are faster and wider than NL jets, and the jet profiles are different: QL jets are distinctly more east-west symmetric than NL jets. Nonetheless, we show in section 6 that the QL jets in Figure 2 do have a small east-west QL asymmetry, and at other points in the (β_*, μ_*)-parameter space, QL jets are strongly east-west asymmetric.

Because the QL jets are faster, the QL system is more zonostrophically unstable than the NL system. In Figures 1 and 2, quasi-steady jets evolve spontaneously from an initially jetless state, as shown in the Hovmöller diagram of the zonal mean flow $U(y,t)$ in Figure 3. Comparing the upper and middle panels in Figure 3, shows that the QL system has significantly longer adjustment times than the NL system.

O'Gorman and Schneider (2007) made the QL approximation (6) in an atmospheric general circulation model and showed by comparison with the full nonlinear version of the model that several important features of the flow are unaffected by complete removal of the eddy-eddy nonlinearity. Comparing Figures 1 and 2 we reach a similar conclusion for the more idealized model studied here. This preliminary conclusion is supported by a detailed comparison between NL and QL solutions in section 6.

There are several ways of motivating QL dynamics. The QL system conserves both energy and enstrophy, and has the same zonal-mean equation and symmetries as the NL system. Thus arguments based on integral invariants apply equally to the QL and the NL system (Salmon 1998). Nonetheless, because EENL is discarded, the QL system cannot exhibit a true Batchelor-Kraichnan inverse energy cascade: in the QL model all nonlinear interactions require participation of the zonal mean flow. Because $U(y,t)$ has a larger length scale than the eddy field, all these nonlinear QL interactions are spectrally nonlocal. Figure 2 shows that the spectrally local Batchelor-Kraichnan inverse cascade is not necessary for zonation. Thus, at the most basic level, the QL system is instructive as an indication of the physically essential processes in zonation.

Stochastic closure versus cumulant expansion

A main motivation of the QL system is that using the statistical method pioneered in meteorology by Farrell and Ioannou (1993b, 2003, 2007) one can compute important average quadratic properties of the QL flow, such as Reynolds stress and the eddy enstrophy and energy. However rather than (6), Farrell and Ioannou (2007) adopt a stochastic closure, which amounts to replacing the eddy-eddy nonlinearity with a combination of random forcing and dissipation:

$$\mathrm{EENL} \to -\xi_{\mathrm{EENL}} + \mu_{\mathrm{EENL}}\zeta'\,; \tag{7}$$

see also DelSole (2001). The intent of (7) is that the random forcing $\xi_{\mathrm{EENL}}(\boldsymbol{x},t)$ and the dissipation $\mu_{\mathrm{EENL}}\zeta'$ should be chosen to match the evolution of the NL system. The terms in (7) then augment the exogeneous forcing and dissipation on the right of (4).

However there is probably no reliable a priori method of determining the right hand side of (7). Heeding the principle to first do no harm, we prefer the QL alternative (6). This has the advantage that one can then make a specific comparison between QL and NL solutions (e.g., as in Figures 1 and 2) and assess the role of EENL.

Our point of view, which follows Marston et al. (2008) and Tobias et al. (2011), is to regard the QL system as an approximation to the NL system. In fact, (6) in tandem with the method of Farrell & Ioannou, is precisely the second-order cumulant expansion CE2 of Marston et al. (2008). It is from this perspective that in section 3 we

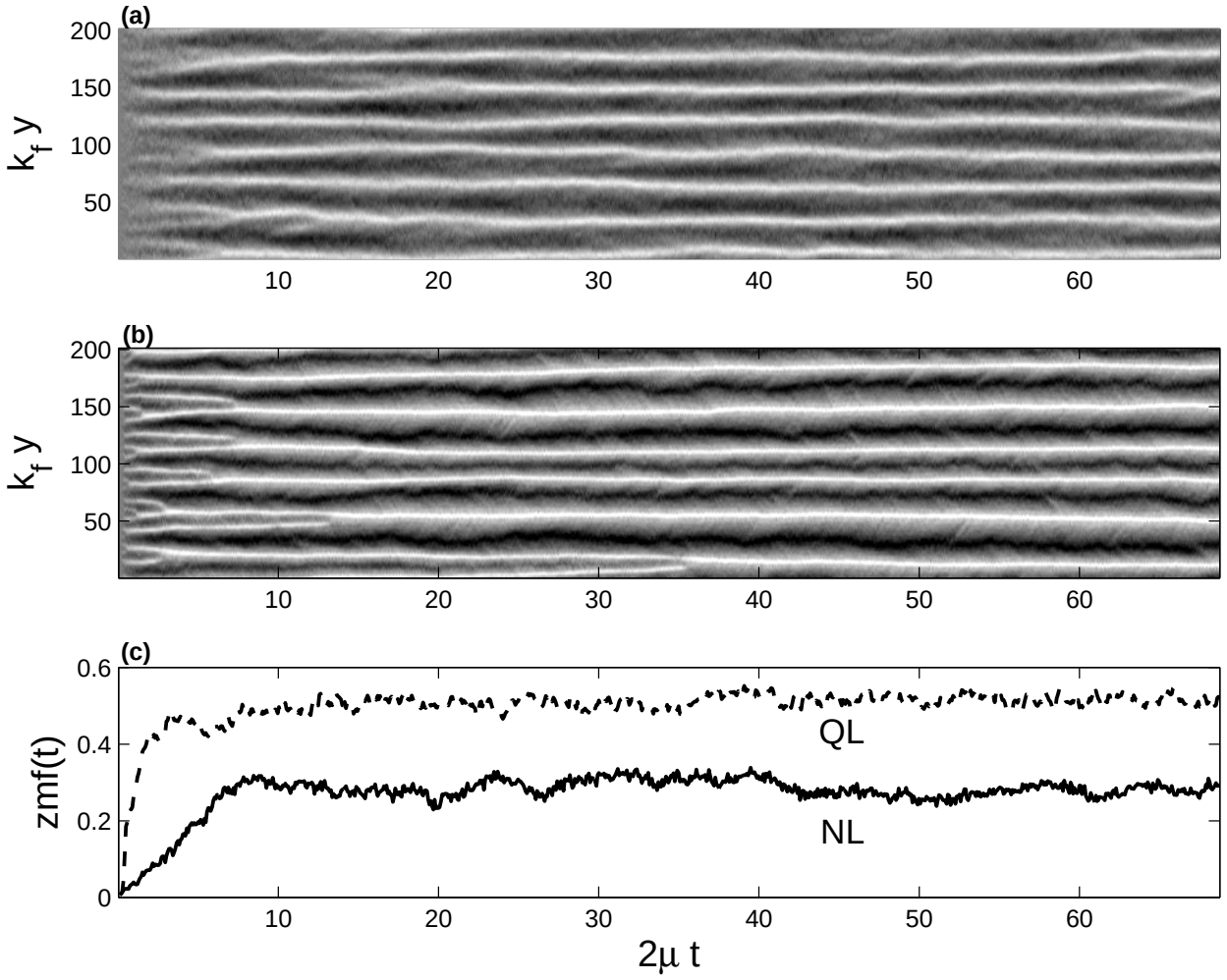

FIG. 3. (a) Hovmöller diagram of the zonal mean velocity $U(y,t)$ obtained by solution of the full nonlinear (NL) system in (1). (b) Hovmöller diagram of the zonal mean velocity $U(y,t)$ obtained by solution of the quasilinear (QL) system. (c) A comparison of the zonal mean energy fraction, $\mathrm{zmf}(t)$ defined in (74), for QL and NL runs. The time-averaged fractions are $\langle \mathrm{zmf} \rangle_{\mathrm{NL}} = 0.3$ and $\langle \mathrm{zmf} \rangle_{\mathrm{QL}} = 0.51$. This figure shows the time evolution of the runs in Figures 1 and 2.

develop a physical-space formulation of CE2, which is suitable for analytic solution.

3. Dynamics of correlations: CE2

In the QL approximation, the eddy vorticity equation can be written as

$$\partial_t \zeta' + \mathsf{L}\, \partial_x \psi' = \xi - \mu\zeta' + \nu\nabla^2\zeta' \,, \tag{8}$$

where L is the Rayleigh-Kuo operator

$$\mathsf{L} \stackrel{\text{def}}{=} U\,\nabla^2 + (\beta - U_{yy}) \,. \tag{9}$$

In this section we obtain a closed deterministic evolution equation for the two-point correlations function of vorticity ζ' and streamfunction ψ'. This correlation equation, (18) below, is coupled to the evolution of the zonal mean flow via the Reynolds stresses, and the Reynolds stresses can be obtained by evaluating derivatives of the correlation function at zero separation. Thus one obtains the zonal-mean evolution equation in (29) below.

Correlation functions: kinematics

We assume that the external forcing $\xi(\boldsymbol{x},t)$ on the right of (8) has a two-point, two-time correlation function of the form

$$\overline{\xi(\boldsymbol{x}_1,t_1)\xi(\boldsymbol{x}_2,t_2)} = \delta(t_2-t_1)\,\Xi(x_1-x_2,y_1,y_2) \,, \tag{10}$$

where the overbar above denotes an ensemble average. The dependence of the spatial correlation function Ξ only on the difference

$$x \stackrel{\text{def}}{=} x_1 - x_2 \tag{11}$$

indicates that the forcing is zonally homogeneous. We do not assume (yet) that the forcing is isotropic and meridionally homogenous.

Notice that that we have changed notation: undecorated x in (11) is the zonal difference coordinate. We also use the shorthand $u_1' = u'(\boldsymbol{x}_1,t)$, $U_2 = U(y_2,t)$, $\zeta_2' = \zeta'(\boldsymbol{x}_2,t)$ etc. Strictly speaking, we should decorate all the variables in (8) with the subscript $n = 1$ or 2 to explicitly indicate whether we refer to the eddy-vorticity equation at the point $\boldsymbol{x}_1 = (x_1,y_1)$, or at the point $\boldsymbol{x}_2 = (x_2,y_2)$. We forbear.

We assume "ergodicity", so that the overbar is also equivalent to the zonal average of a single realization. We desire the single-time two-point correlation functions

$$\mathcal{Z}(x,y_1,y_2,t) \stackrel{\text{def}}{=} \overline{\zeta_1'\zeta_2'} \,, \tag{12}$$

and

$$\Psi(x,y_1,y_2,t) \stackrel{\text{def}}{=} \overline{\psi_1'\psi_2'} \,. \tag{13}$$

Because derivatives commute with the ensemble average, the two correlation functions above are related by

$$\mathcal{Z} = \nabla_1^2\nabla_2^2\Psi \,, \tag{14}$$

where the Laplacian acting on the coordinates of point n is

$$\nabla_n^2 \stackrel{\text{def}}{=} \partial_x^2 + \partial_{y_n}^2 \,. \tag{15}$$

Given the streamfunction correlation $\Psi(x,y_1,y_2,t)$, one can obtain the velocity correlation tensor as

$$V_{ij}(x,y_1,y_2,t) \stackrel{\text{def}}{=} \begin{pmatrix} \overline{u_1'u_2'} & \overline{u_1'v_2'} \\ \overline{u_2'v_1'} & \overline{v_1'v_2'} \end{pmatrix} = \begin{pmatrix} \partial_{y_1}\partial_{y_2} & \partial_x\partial_{y_1} \\ -\partial_x\partial_{y_2} & -\partial_x^2 \end{pmatrix} \Psi \,. \tag{16}$$

Because the choice of denoting one point as $\boldsymbol{x}_1$ and the other as $\boldsymbol{x}_2$ is arbitrary, all correlation function have an important "exchange" symmetry

$$\Psi(x,y_1,y_2) = \Psi(-x,y_2,y_1) \,, \tag{17}$$

and likewise for $\mathcal{Z}$, Ξ etc.

Correlation functions: dynamics

It follows from (8) and (10) that the correlation functions evolve as

$$\partial_t\mathcal{Z} + \left(\nabla_2^2\mathsf{L}_1 - \nabla_1^2\mathsf{L}_2\right)\partial_x\Psi = \Xi - 2\mu\mathcal{Z} + \nu\left(\nabla_1^2+\nabla_2^2\right)\mathcal{Z} \,, \tag{18}$$

where the Rayleigh-Kuo operator at point n is $\mathsf{L}_n \equiv U_n\,\nabla_n^2 + (\beta - U_n'')$.

To derive (18), multiply the equation for $\partial_t\zeta_1'$ by ζ_2' and add this to the $\partial_t\zeta_2'$-equation multiplied by ζ_2'. The sum is then ensemble averaged, and after the average all fields depend on x_1 and x_2 only through the combination $x = x_1 - x_2$. Because of this zonal homogeneity $\partial_{x_1} = -\partial_{x_2} = \partial_x$. Thus, for example,

$$\overline{\zeta_2'\mathsf{L}_1\partial_{x_1}\psi_1'} + \overline{\zeta_1'\mathsf{L}_2\partial_{x_2}\psi_2'} = \left(\nabla_2^2\mathsf{L}_1 - \nabla_1^2\mathsf{L}_2\right)\partial_x\,\overline{\psi_1'\psi_2'} \,. \tag{19}$$

A crucial simplification is that the forcing is rapidly decorrelating in time, as expressed by the $\delta(t_1-t_2)$ in (10). Considerations summarized in Appendix B (amounting to a simple proof of Ito's formula) show that

$$\overline{\zeta_1'\xi_2} + \overline{\zeta_2'\xi_1} = \Xi \,. \tag{20}$$

The result above is the origin of the first term on the right hand side of (18).

Collective coordinates

As alternatives to y_1 and y_2, there are advantages in using the "collective coordinates"

$$y \stackrel{\text{def}}{=} y_1 - y_2 \qquad \text{and} \qquad \bar{y} \stackrel{\text{def}}{=} \tfrac{1}{2}(y_1+y_2) \,. \tag{21}$$

Eventually we will restrict attention to homogenous and isotropic forcing, and at that point we take Ξ in (10) to be a function only of the two-point separation

$$r \stackrel{\text{def}}{=} |\boldsymbol{x}_1 - \boldsymbol{x}_2| = \sqrt{x^2+y^2} \,. \tag{22}$$

Collective coordinates are then essential for analytic progress.

In terms of y and $\bar{y}$, the Laplacians are

$$\nabla_n^2 = \nabla^2 - (-1)^n \partial_y \partial_{\bar{y}} + \tfrac{1}{4}\partial_{\bar{y}}^2 \,, \tag{23}$$

where $\nabla^2 \stackrel{\text{def}}{=} \partial_x^2 + \partial_y^2$ is the "separation" Laplacian. Thus, for instance,

$$\mathcal{Z} = \left(\nabla^2 + \partial_y\partial_{\bar{y}} + \tfrac{1}{4}\partial_{\bar{y}}^2\right)\left(\nabla^2 - \partial_y\partial_{\bar{y}} + \tfrac{1}{4}\partial_{\bar{y}}^2\right)\Psi \,, \tag{24}$$

$$= \nabla^4\Psi + \tfrac{1}{2}\left(\partial_x^2 - \partial_y^2\right)\partial_{\bar{y}}^2\Psi + \tfrac{1}{16}\partial_{\bar{y}}^4\Psi \,. \tag{25}$$

Using the coordinates in (21), the correlation equation (18) becomes

$$\partial_t\mathcal{Z} + (U_1 - U_2)\partial_x\mathcal{Z} - (U_1'' - U_2'')\left(\nabla^2 + \tfrac{1}{4}\partial_{\bar{y}}^2\right)\partial_x\Psi - (2\beta - U_1'' - U_2'')\,\partial_{\bar{y}}\partial_y\partial_x\,\Psi = \Xi - 2\mu\mathcal{Z} + 2\nu\nabla^2\mathcal{Z} + \tfrac{1}{2}\nu\partial_{\bar{y}}^2\mathcal{Z} \,, \tag{26}$$

where now $U_1 = U\left(\bar{y} + \frac{1}{2}y\right)$ and $U_2 = U\left(\bar{y} - \frac{1}{2}y\right)$

The zonal mean flow equation

One advantage of collective coordinates is that mean square quantities, such as the enstrophy, are obtained by evaluating correlation functions at zero separation i.e., by setting $(x, y) = 0$. For example if one possesses $\mathcal{Z} = \mathcal{Z}(x, y, \bar{y}, t)$ then the eddy enstrophy is $\overline{\zeta'^2} = \mathcal{Z}(0, 0, \bar{y}, t)$.

A key result, obtained by evaluating

$$\overline{u_1'v_2'} + \overline{u_2'v_1'} = 2\partial_x\partial_y\Psi \tag{27}$$

at $(x, y) = 0$, is that the Reynolds stress is

$$\overline{u'v'}(\bar{y}, t) = \partial_y\partial_x\Psi(0, 0, \bar{y}, t) \,. \tag{28}$$

Thus the mean flow equation (3) can be written as

$$\partial_t U + \partial_{\bar{y}}\partial_y\partial_x\Psi(0, 0, \bar{y}, t) = -\mu U + \nu\partial_{\bar{y}}^2 U \,. \tag{29}$$

The mean flow equation (29), coupled with the correlation equation (26), is a closed system for the ensemble-averaged properties of QL dynamics.

4. Zonostrophic instability of a spatially homogeneous and isotropic base-state flow

The spatially homogeneous basic state

We now suppose that the forcing is statistically homogenous and isotropic, *i.e.* that the correlation function of the forcing has the particular form

$$\overline{\xi(\boldsymbol{x}_1, t_1)\xi(\boldsymbol{x}_2, t_2)} = \delta(t_2 - t_1)\,\Xi(r) \,, \tag{30}$$

where r is the two-point separation defined in (22). Because Ξ does not depend on $\bar{y}$, there is a simple exact solution to (26) and (29). This solution is spatially homogeneous and isotropic and has no mean flow, $U = 0$. With these simplifications the correlation equation (26) collapses to:

$$\left(2\mu - 2\nu\nabla^2\right)\mathcal{Z}_{\mathsf{H}} = \Xi \,. \tag{31}$$

The subscript H emphasizes that $\mathcal{Z}_{\mathsf{H}}(r)$ is spatially homogeneous i.e., independent of $\bar{y}$. The streamfunction correlation function, $\Psi_{\mathsf{H}}(x, y)$, can be obtained from $\mathcal{Z}_{\mathsf{H}}$ by solving $\nabla^4\Psi_{\mathsf{H}} = \mathcal{Z}_{\mathsf{H}}$. It is remarkable that $\mathcal{Z}_{\mathsf{H}}$ in (31) is independent of β: an isotropic and spatially homogenous forcing drives an isotropic and spatially homogeneous flow, despite the anisotropy of Rossby wave propagation.

We now apply the Fourier integral theorem,

$$\tilde{f}(p, q) \stackrel{\text{def}}{=} \iint f(x, y)\mathrm{e}^{-i(px+qy)}\,\mathrm{d}x\,\mathrm{d}y \,, \tag{32}$$

$$f(x, y) = \iint \tilde{f}(p, q)\mathrm{e}^{i(px+qy)}\,\frac{\mathrm{d}p\,\mathrm{d}q}{(2\pi)^2} \,, \tag{33}$$

to (31). We use the notation

$$h \stackrel{\text{def}}{=} \sqrt{p^2 + q^2} \,, \tag{34}$$

so that after the Fourier transform $h^4\tilde{\Psi}_{\mathsf{H}} = \tilde{\mathcal{Z}}_{\mathsf{H}}$, and the streamfunction spectrum is related to the forcing spectrum by

$$\tilde{\Psi}_{\mathsf{H}}(p, q) = \frac{\tilde{\Xi}(p, q)}{2\mu h^4 + 2\nu h^6} \,. \tag{35}$$

We emphasize that $\tilde{\Psi}_{\mathsf{H}}(p, q)$ in (35) is not singular as $h \to 0$. Specifically, the vorticity forcing ξ on the right of (8) is the curl of a solenoidal random force in the momentum equation i.e., $\xi = \nabla^2 a$, where $a(\boldsymbol{x}, t)$ is a spatially homogeneous and stationary random process. Thus, in analogy with (30),

$$\overline{a(\boldsymbol{x}_1, t_1)a(\boldsymbol{x}_2, t_2)} = \delta(t_2 - t_1)A(r) \,, \tag{36}$$

and therefore $\Xi = \nabla^4 A$. In terms of A, the streamfunction spectrum in (35) becomes

$$\tilde{\Psi}_{\mathsf{H}}(p, q) = \frac{\tilde{A}(p, q)}{2\mu + 2\nu h^2} \,. \tag{37}$$

Since $a(\boldsymbol{x}, t)$ is stationary, the spectra $\tilde{A}(p, q)$ and $\tilde{\Psi}_{\mathsf{H}}(p, q)$ are finite as $h \to 0$ (provided that $\mu \neq 0$).

Later we will need two integral constraints on the vorticity forcing correlation function Ξ:

$$\iint \Xi(x, y)\,\mathrm{d}x\mathrm{d}y = \tilde{\Xi}(0, 0) = 0 \,, \tag{38}$$

and also

$$\iint \Xi(x, y)r^2\,\mathrm{d}x\mathrm{d}y = \lim_{h\to 0} h^{-2}\tilde{\Xi}(p, q) = 0 \,. \tag{39}$$

These follow from $\Xi = \nabla^4 A$, and the assumption that the correlation function $A(r)$ in (36) decays faster than r^{-1} as $r \to \infty$. The constraints above are satisfied by the standard forcing protocol described in Appendix A, which has zero spectral density around $h = 0$.

The dispersion relation of inviscid and isotropic flow

The linear stability of the spatially homogeneous solution in (37) is determined by imposing small initial disturbances and examining evolution in time. The perturbation variables are added to the base state variables, $(0, \Psi_{\mathsf{H}}, \mathcal{Z}_{\mathsf{H}})$ and substituted into equations (26) and (29). The total 'flow', with mean and imposed small perturbations, is

$$\begin{bmatrix} U(\bar{y},t) \\ \mathcal{Z}(x,y,\bar{y},t) \\ \Psi(x,y,\bar{y},t) \end{bmatrix} = \begin{bmatrix} 0 \\ \mathcal{Z}_{\mathsf{H}}(x,y) \\ \Psi_{\mathsf{H}}(x,y) \end{bmatrix} + \mathrm{e}^{im\bar{y}+st} \begin{bmatrix} \hat{U}(m,s) \\ \hat{\mathcal{Z}}(x,y;m,s) \\ \hat{\Psi}(x,y;m,s) \end{bmatrix} + \text{c.c.}\,, \tag{40}$$

where m is the meridional wavenumber of the disturbances and s is the growth rate, with growing perturbations corresponding to $\Re(s) > 0$. Retaining terms linear in the perturbation variables $(\hat{U}, \hat{\Psi}, \hat{\mathcal{Z}})$, one has the equations governing the evolution of small perturbations to the homogeneous solution. The details of the subsequent solution are in Appendix C, and a main result of that analysis is the dispersion relation

$$2\mu\beta^2 \, \frac{s+\mu}{s+2\mu} = \int_0^\infty h^5 \left(h^2 - m^2\right) \tilde{A}(h) \, Q\left[\frac{h^2(s+2\mu)}{m\beta}, \frac{m}{h}\right] \frac{\mathrm{d}h}{2\pi}\,, \tag{41}$$

where $\tilde{A}(h)$ is the forcing spectrum in (37), and the function $Q(\chi, n)$ is defined by the angular integral

$$Q(\chi,n) \stackrel{\text{def}}{=} \oint \frac{\cos^2\theta \, \left(1 + n^2 - 4\sin^2\theta\right)}{\left(\chi + \mathrm{i}\sin 2\theta\right)^2 + n^2\left[\chi^2(n^2 + 2 - 4\sin^2\theta) + \cos^2\theta\right]} \frac{\mathrm{d}\theta}{2\pi}\,. \tag{42}$$

The dispersion relation (41) applies to the special case of isotropic forcing, $A = A(r)$ and $\nu = 0$; a more general expression of the dispersion relation is in Appendix C.

Dr. George Carnevale has shown that the dispersion relation in (41) and (42) is also obtained from equation (5.13) in Carnevale and Martin (1982). The field-theoretic approach of Carnevale and Martin (1982) is different from the approximation used to obtain the CE2 system in (26) and (29) e.g., CE2 contains terms such as $(U_1 - U_2)\mathcal{Z}_x$, which Carnevale and Martin (1982) consider to be fourth order in wave amplitude, and therefore negligible. However, after linearization of CE2 around a basic state with $U = 0$, these terms are neglected. Therefore the linearized version of CE2 in this section is equivalent to the weak-turbulence limit (5.13) in Carnevale and Martin (1982). This consistency provides confidence in (41) and (42).

Ring forcing

In most previous investigations of zonation, the forcing is limited to an annulus of wave numbers in Fourier-space. Typically the annulus of forced modes has a mean radius $h = k_f$ and has thickness $2\delta k \ll k_f$. This is the "narrow-band forcing" described in Appendix A. We idealize this choice further by considering 'ring' forcing corresponding to the limit $\delta k \to 0$. In other words, we consider a random flow, driven isotropically by injecting energy on the circle $h = k_f$ in wavenumber space. This corresponds to

$$A(r) = \frac{2\varepsilon}{k_f^2} J_0(k_f r)\,, \qquad \tilde{A}(h) = \frac{4\pi\varepsilon}{k_f^3}\delta(h - k_f)\,, \tag{43}$$

where J_0 is the Bessel function of order zero. Notice that $\Xi = \nabla^4 A = k_f^4 A$. With $\nu = 0$ — as we assume in (41) — the spatially homogeneous base state solution in (37) is

$$\Psi_{\mathsf{H}}(r) = \varepsilon \, \frac{J_0(k_f r)}{k_f^2 \mu}\,, \qquad \tilde{\Psi}_{\mathsf{H}}(h) = 2\pi\varepsilon \, \frac{\delta(h - k_f)}{k_f^3 \mu}\,. \tag{44}$$

The parameter ε above, with dimensions Watts per kilogram, is the rate of working of the force that sustains the base state (44) flow against dissipation.

With $\delta(h - k_f)$ in (43), the h-integral in (41) is trivial. Before proceeding however, it is convenient to write the various parameters in the non-dimensional form using the length scale k_f^{-1} and time scale $(\varepsilon k_f^2)^{-1/3}$. These scales lead to the control parameters

$$\mu_* \stackrel{\text{def}}{=} \frac{\mu}{k_f^{2/3}\varepsilon^{1/3}}\,, \qquad \beta_* \stackrel{\text{def}}{=} \frac{\beta}{k_f^{5/3}\varepsilon^{1/3}}\,. \tag{45}$$

The nondimensional wavenumber and growth rate are

$$m_* \stackrel{\text{def}}{=} \frac{m}{k_f}\,, \quad \text{and} \quad s_* \stackrel{\text{def}}{=} \frac{s}{(\varepsilon k_f^2)^{1/3}}\,. \tag{46}$$

The zonostrophic dispersion relation in non-dimensional variables is then

$$\mu_*\beta_*^2 \left(\frac{s_* + \mu_*}{s_* + 2\mu_*}\right) = (1 - m_*^2)\, Q\left(\frac{s_* + 2\mu_*}{m_*\beta_*}, m_*\right)\,, \tag{47}$$

with the function Q defined in (42). We now lighten the notation by dropping the $*$ on non-dimensional variables m and s. We have obtained the growth rate by solving (47) numerically for $s = s_r + is_i$. This numerical solution indicates that modes with $s_r > 0$ are found only if $0 < m^2 < 1$, and these unstable modes have $s_i = 0$. We have been unable to obtain a satisfactory non-numerical proof of these two important properties of zonostrophic instability.

Figure 4 shows some examples of the growth rate $s(m)$ plotted as a function of m for various values of β_*, with $\mu_* = 0.15$ in all cases. If $s > 0$ for some values of m (e.g., $\beta_* = 0.15$ and 1 in Figure 4) then the homogeneous flow is unstable and zonal jets will grow from very small initial amplitude. Also shown in Figure 4 are two marginally stable situations $\beta_* = 0.0634$ and $\beta_* = 2.571$. These are defined

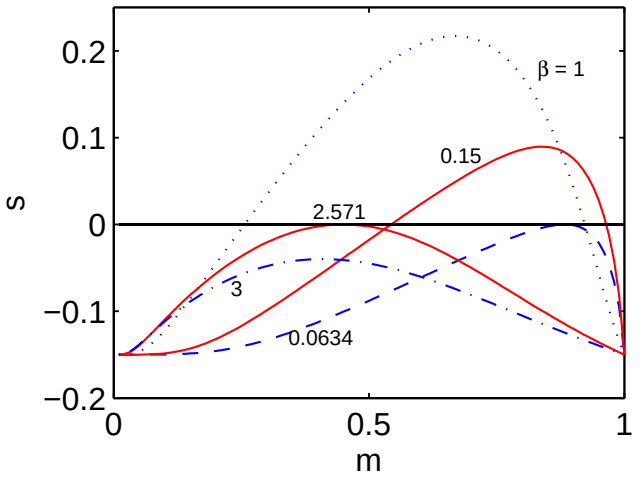

FIG. 4. The growth rate s as a function of m for $\mu_* = 0.15$ and five values of β_* indicated on the curves. The variables in this figure are non-dimensionalized according to (45) and (46). These modes have $s_i = 0$ i.e., s is real. The curves $\beta_* = 2.571$ and 0.0634 correspond to the marginally stable situation defined by (48).

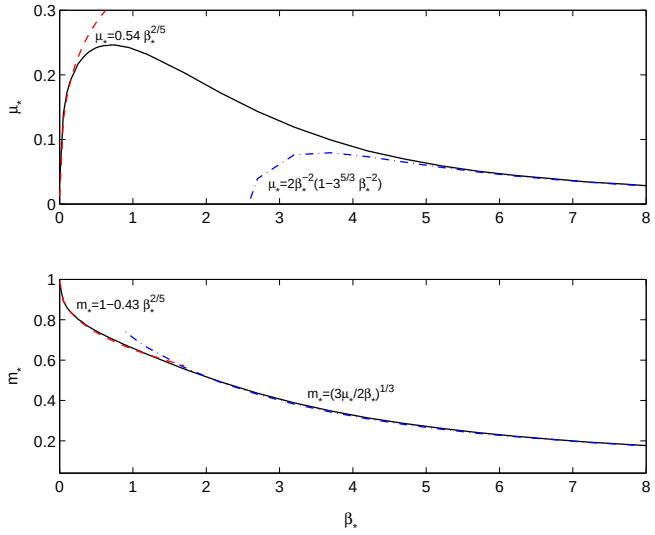

FIG. 5. The top panel is the critical curve, $\mu_*^{\rm c}(\beta_*)$; linear zonostrophic instability occurs in the region below the critical curve. The bottom panel shows the wavenumber on the critical curve, $m^{\rm c}(\beta_*)$ i.e., the most linearly unstable wavenumber. Asymptotic approximations for the critical curve and the most unstable wavenumber based on $\beta_* \gg 1$ (dash-dot) and $\beta_* \ll 1$ (dash) are shown in both panels.

by the condition that the most unstable disturbance has $s = 0$:

$$\max_{\forall m} s(m;\beta_*,\mu_*) = 0\,. \tag{48}$$

A main conclusion resulting from our analysis is that zonostrophic instability is suppressed if β_* is either too large or too small e.g., in Figure 4 the flow is stable if $\beta_* > 2.571$ or if $\beta_* < 0.0634$.

The marginal stability condition in (48), which is equivalent to the requirements

$$s(m;\beta_*,\mu_*) = 0\,, \quad \text{and} \quad \partial_m s(m;\beta_*,\mu_*) = 0\,, \tag{49}$$

defines a "critical curve" in the (β_*,μ_*)-parameter plane. This curve, $\mu_* = \mu_*^{\rm c}(\beta_*)$ is shown in the upper panel of Figure 5. The solution $(\mathcal{Z},U) = (\mathcal{Z}_{\rm H},0)$ is linearly unstable in the region below the critical curve. The peak of the critical curve is $0.2464 = \mu_*^{\rm c}(0.65)$. This peak defines the "most unstable" point in the (β_*,μ_*)-parameter space i.e., the largest value of drag μ_* at which the homogeneous solution loses stability. The lower panel of Figure 5 shows the wavenumber $m^{\rm c}(\beta_*)$ of the incipient instability i.e., the wavenumber determined by simultaneously satisfying the two equations in (49).

Approximations to the neutral curve with large and small β_*

Also shown in Figure 5 are analytic approximations in the complementary limits $\beta_* \ll 1$ and $\beta_* \gg 1$. These results are obtained via asymptotic analysis of the integral $Q(\chi,n)$ in (42), and simplification of the dispersion relation (47) (see Appendix E). If $\beta_* \ll 1$ then the critical curve is

$$\mu_*^{\rm c}(\beta_*) = \left(\frac{3}{64}\right)^{1/5} \beta_*^{2/5} + O\left(\beta_*^{4/5}\right)\,, \tag{50}$$

with wavenumber

$$m^{\rm c}(\beta_*) = 1 - 0.43\beta_*^{2/5} + O\left(\beta_*^{4/5}\right)\,. \tag{51}$$

In the complementary limit $\beta_* \gg 1$, the approximation to the critical curve is

$$\mu_*^{\rm c}(\beta_*) = \frac{2}{\beta_*^2}\left(1 - \frac{3^{5/3}}{\beta_*^2}\right) + O\left(\beta_*^{-6}\right)\,, \tag{52}$$

with wavenumber

$$m^{\rm c}(\beta_*) = \frac{3^{1/3}}{\beta_*} + O\left(\beta_*^{-3}\right)\,. \tag{53}$$

The lower panel of Figure 5 shows that linear zonostrophic instability is spectrally nonlocal only in the limit $\beta_* \to \infty$: in that case the most unstable wavenumber is much less than the forced wavenumber k_f, implying a scale separation between the scales at which energy is injected and the scale at which jets initially form. In the other limit $\beta_* \to 0$ the linearly unstable wavenumber is close to k_f.

The small wavenumber structure of the growth rate

The structure of the dispersion relation at small m provides insight into the nature of zonostrophic instability. Looking at Figure 4, we anticipate that

$$s = -\mu_* + \eta_2 m^2 + \eta_4 m^4 + O\left(m^6\right) , \tag{54}$$

where $\eta_2 > 0$ might explain the increase in s that results in the instability with $s > 0$. This would be a "negative-viscosity instability", which is the interpretation offered by Farrell and Ioannou (2007) and Bakas and Ioannou (2011a,b).

However there is a small surprise: from (E18) we find that the expansion of the dispersion relation (47) around $m = 0$ is:

$$s = -\mu_* + \frac{3\beta_*^2}{8\mu_*^4}\, m^4 + O\left(m^6\right) . \tag{55}$$

i.e., the term η_2 in (54), corresponding to viscosity, is identically zero. Instead, the instability is associated with a destabilizing *hyperviscous* term i.e., the Reynolds stresses are related to the zonal mean flow by

$$\overline{u'v'} = -\frac{3\beta_*^2}{8\mu_*^4}\,\frac{\partial^3 U}{\partial y^3} , \tag{56}$$

leading to the small-m growth rate in (55). We analyze this curious situation further in Section 5 and show that $\eta_2 = 0$ follows from the assumed isotropy of the forcing i.e., $\eta_2 = 0$ is not a special property of the particular model in (44). The conclusion is that zonostrophic instability requires anti-frictional momentum fluxes, and in the small-m limit this anti-friction is hyerviscous.

In recent work Bakas and Ioannou (2011a,b) reach a different conclusion viz., that the anti-frictional effect resulting in nonzero Reynolds stress is equivalent to non-zero and positive η_2, and that the hyper-viscous coefficient η_4 is negative and therefore stabilizing. We believe that these differences may result from a different choice of forcing Ξ. Bakas and Ioannou (2011a,b) use an anisotropic forcing, while our conclusion above is specifically for isotropic forcing. The importance of isotropy to our conclusion is underscored in the section 5.

5. Isotropy and zero eddy viscosity

In the discussion surrounding (55) we observed that the term in the zonostrophic dispersion relation corresponding to the eddy viscosity is zero. This result emerges from the analysis of a complicated dispersion relation and surely deserves a more fundamental explanation, or at least another explanation. Thus in this section we more directly obtain the eddy viscosity of an isotropically forced QL β-plane shear flow, and show that the result is identically zero.

The eddy viscosity is obtained by calculating the Reynolds stresses in a situation where there is good scale separation between a shear flow and eddies. The best possible scale separation is achieved by considering a Couette flow, $U_n = \gamma y_n$, and in this case the CE2 correlation equation (26) collapses to

$$\gamma y \partial_x \mathcal{Z} - 2\beta \partial_{\bar{y}} \partial_x \partial_y \Psi = \Xi(x,y) - 2\mu \mathcal{Z} . \tag{57}$$

For the moment we assume general forcing i.e., there is no restriction to isotropic forcing (yet).

The eddy viscosity $\nu_{\rm e}$ is defined by the relation

$$\nu_{\rm e} \stackrel{\rm def}{=} -\gamma^{-1}\,\overline{u'v'} . \tag{58}$$

The goal is to solve (57) and obtain the Reynolds stress $\overline{u'v'}$ by evaluating Ψ_{xy} at zero separation e.g., as in (28). The eddy viscosity then follows from the definition (58).

We expect that $\nu_{\rm e}$ defined above is equal to the coefficient η_2 in (54). In the $m \to 0$ limit, the modal solution in (40) varies on the length scale m^{-1}, which is much greater than the length scale of the forcing, viz., k_f^{-1}. Thus on the scale of the forcing, the growing zonal disturbance resembles the Couette flow[1] (except at the "shearless" points, where $U_y = 0$). By calculating the Reynolds stress in this situation one can anticipate the low-wavenumber structure of the dispersion relation. This reasoning is identical to methods in kinetic theory by which the molecular shear viscosity is calculated.

A solution of the correlation equation

We can simplify (57) with $\mathcal{Z} = \mathcal{Z}(x,y)$ i.e., by looking for a solution independent of $\bar{y}$:

$$\gamma y \partial_x \mathcal{Z} = \Xi(x,y) - 2\mu \mathcal{Z} . \tag{59}$$

This reduction is surprising because the β-effect is removed from the problem. Equation (59) can be solved straightforwardly as an ordinary differential equation in x. However to make contact with a large literature on sheared disturbances, it is instructive to consider the initial value problem

$$F_t + \gamma y \partial_x F = -2\mu F , \tag{60}$$

with the initial condition

$$F(x,y,0) = \Xi(x,y) . \tag{61}$$

The solution of the steady problem (59) is then obtained as

$$\mathcal{Z}(x,y) = \int_0^\infty F(x,y,t)\,{\rm d}t . \tag{62}$$

Thus, solving the initial value problem for F, the vorticity correlation function is written as the time integral of a sheared disturbance:

$$\mathcal{Z}(x,y) = \int_0^\infty {\rm e}^{-2\mu t}\,\Xi\left(x-\gamma t y, y\right)\,{\rm d}t . \tag{63}$$

[1] There is also uniform advection by the zonal flow. But that sweeping is eliminated by the difference $U_1 - U_2$ in the correlation equation (26), and is therefore inconsequential to Reynolds stresses.

The Reynolds stresses

To obtain the correlation function Ψ from $\mathcal{Z}$ we must solve the two-dimensional biharmonic equation $\nabla^4\Psi = \mathcal{Z}$, which is accomplished with the Green's function defined by $\nabla^4 G = \delta(x)\delta(y)$, or $\tilde{G}(h) = h^{-4}$, or

$$G(x,y) = \frac{r^2}{8\pi}\left(\ln r - 1\right) . \tag{64}$$

With $G(x,y)$ in hand, we have

$$\Psi(x,y) = \iint G(x-x',y-y')\mathcal{Z}(x',y')\,\mathrm{d}x'\mathrm{d}y' . \tag{65}$$

The Reynolds stress now follows by evaluating Ψ_{xy} at zero separation, or

$$\overline{u'v'} = \frac{1}{4\pi}\iint \frac{xy}{x^2+y^2}\,\mathcal{Z}(x,y)\,\mathrm{d}x\,\mathrm{d}y . \tag{66}$$

This is a very convenient and general expression for the Reynolds stresses $\overline{u'v'}$ in terms of the vorticity correlation function $\mathcal{Z}(x,y)$.

Substituting (63) into (66) results in a triple integral. To disentangle this, exchange the order so that t-integral is last, and in the inner x and y integrals "unshear" the correlation function with the coordinate change

$$x_1 = x - \gamma y t\,, \qquad y_1 = y\,. \tag{67}$$

After these maneuvers the Reynolds stress is

$$\overline{uv} = \frac{1}{4\pi}\int_0^\infty \mathrm{e}^{-2\mu t}\Sigma(t)\,\mathrm{d}t\,, \tag{68}$$

where

$$\Sigma(t) \stackrel{\text{def}}{=} \iint \frac{(x_1+\gamma t y_1)y_1}{(x_1+\gamma t y_1)^2+y_1^2}\,\Xi\left(x_1,y_1\right)\,\mathrm{d}x_1\mathrm{d}y_1 . \tag{69}$$

Now we restrict attention to isotropic forcing i.e.,

$$\Xi(x_1,y_1) = \Xi\left(\sqrt{x_1^2+y_1^2}\right) . \tag{70}$$

Then in polar coordinates, the double integral in (69) factors:

$$\begin{aligned}\Sigma(t) &= \oint \frac{(\cos\theta+\gamma t\sin\theta)\sin\theta}{(\cos\theta+\gamma t\sin\theta)^2+\sin^2\theta}\,\mathrm{d}\theta \times \int_0^\infty \Xi(r) r\mathrm{d}r\,,\\ &= \frac{2\pi\,\gamma t}{4+(\gamma t)^2} \times \int_0^\infty \Xi(r)\,r\mathrm{d}r\,,\\ &= 0\,.\end{aligned} \tag{71}$$

The final line follows from the constraint (38), and implies that $\overline{u'v'} = 0$. That is, the eddy viscosity ν_e is zero.

We remark that the constraints in (38) and (39) are required so that correlation function Ψ on the left of (65) decays as $r \to \infty$, despite the $r \to \infty$ divergence of the Green's function $G(r)$ in (64). In the convolution integral on the right of (65), the large-r divergence of G is shielded by zero integrals of the vorticity correlation function $\mathcal{Z}$, which follows from the integral constraints on Ξ in (38) and (39).

There are two important caveats associated with the conclusion that $\nu_\mathrm{e} = 0$: the stochastic forcing is isotropic and dissipation is provided only by Ekman drag. Relaxing either or both of these assumptions might result in non-zero ν_e.

The kinetic energy density

The energy power integral for the β-plane Couette flow problem considered here is obtained by first rewriting (59) as

$$\gamma\nabla^2\left(y\nabla^2\partial_x\Psi - 2\partial_x\partial_y\Psi\right) = \nabla^4 A - 2\mu\nabla^4\Psi\,. \tag{72}$$

Canceling a Laplacian, and evaluating the result at zero separation, one obtains[2]

$$\gamma\overline{u'v'} = \varepsilon - \mu\left(\overline{u'^2}+\overline{v'^2}\right) . \tag{73}$$

The left hand side is the transfer of energy between the eddies and the Couette flow, which is zero because $\overline{u'v'} = 0$. Therefore the statistically energy balance is between dissipation due to drag and the rate of working of the random force that drives the eddies. Remarkably, because the Reynolds stresses are zero, the eddy kinetic energy of the statistically steady flow is $\varepsilon/(2\mu)$, independent of both β and γ.

Discussion

To a certain extent the result $\nu_\mathrm{e} = 0$ is anticipated in the literature on sheared disturbances. Shepherd (1985) showed that an isotropic initial distribution of Rossby waves maintains a constant energy density, despite shearing by a Couette flow; see also Farrell and Ioannou (1993a) and Holloway (2010). The solution in (63), with the isotropic initial condition in (61), is essentially a time integral of Shepherd's solution of the sheared-disturbance problem with an isotropic initial condition.

Via direct numerical simulation (but with $\beta = 0$), Cummins and Holloway (2010) have recently shown that the eddy-eddy nonlinearity, EENL, is essential in producing nonzero Reynolds stresses from Couette-sheared eddies. Cummins and Holloway (2010) identify the essential role of EENL as restoration of isotropy at high wavenumbers. Moreover, as a result of nonlinearly restored isotropy, the eddy viscosity ν_e is robustly *positive*, and thus cannot serve as an explanation of zonostrophic instability. Whatever the sign

[2]The rate of energy injection is $\varepsilon = -\frac{1}{2}\nabla^2 A|_0$; see, for example, the model forcing in(43).

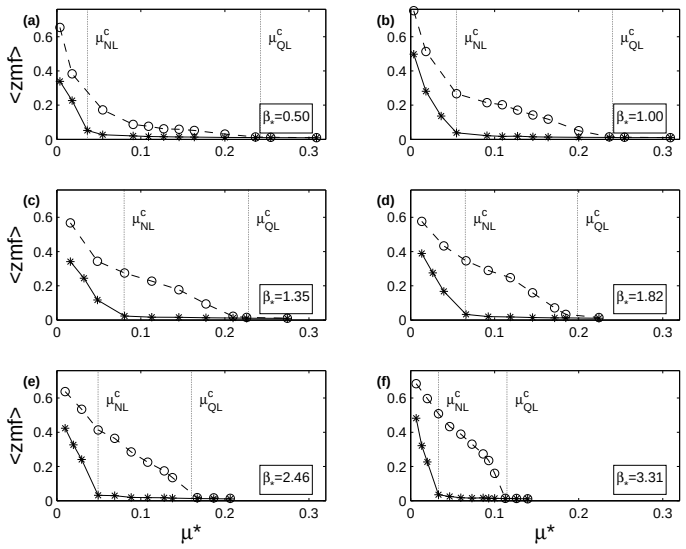

FIG. 6. The time-averaged zonal mean energy fraction $\langle \mathrm{zmf} \rangle$ as a function of μ_*, with β_* fixed as indicated in the bottom right corner of each panel. QL simulations are indicated by $\circ$ and NL solutions by $*$.

of ν_e, an unfortunate consequence of (6) is that restoration of isotropy at small scales is absent in QL dynamics, and not represented in the ensemble-averaged dynamics CE2.

6. Zonation in QL and NL solutions

We now turn to numerical solutions for a comparison between the full nonlinear system, the quasilinear system and the predictions of CE2. In these calculations the resolution is 512×512, and we use the ETDRK4 time-stepping scheme (Cox and Matthews 2005). In addition to the control parameters β_* and μ_* defined in (45), there is a third control parameter which is the size of the domain relative to the forced wavenumber k_f: in our computations the domain is a doubly periodic square $2\pi L \times 2\pi L$, with $k_f L = 32$. Thus there is scale separation between the forcing and the domain.

We have obtained about 150 QL and NL numerical solutions, with the planetary vorticity gradient in the range

$$0.1 \leq \beta_* \leq 3.3\,,$$

and the drag parameter in the range

$$0.0051 \leq \mu_* \leq 0.309\,.$$

In this section we use these solutions to compare QL and NL solutions, and assess the validity of the CE2 linear stability analysis.

The onset of zonation in NL and QL solutions

Shown in the bottom panel of Figure 3 is the evolution of the fraction of kinetic energy in the zonal mean flow,

$$\mathrm{zmf}(t) \stackrel{\mathrm{def}}{=} \frac{\int U^2 \,\mathrm{d}a}{\int U^2 + u'^2 + v'^2 \,\mathrm{d}a}\,. \tag{74}$$

$\int \cdots \mathrm{d}a$ above denotes the area integral over the entire domain. The index $\mathrm{zmf}(t)$ is a gross measure of the strength of the zonal mean flow. The time average, denoted by $\langle \mathrm{zmf} \rangle$, is computed by averaging over an interval $t_1 < t < t_1 + 10/\mu$, where typically $2\mu t_1 > 40$. This long spin-up ensures that statistical equilibrium has been achieved and is consistent with the equilibration time suggested by Galperin et al. (2006).

The index $\langle \mathrm{zmf} \rangle$ is used to classify the flow. Figure 6 summarizes a suite of QL and NL calculations in which the drag parameter μ_* is varied at fixed β_*. The onset of zonation is indicated by the increase in $\langle \mathrm{zmf} \rangle$. The dotted lines marked μ^c_{QL} correspond to the critical curve in the upper panel of figure 5; these analytic predictions compare well with the increase in $\langle \mathrm{zmf} \rangle$ in the QL numerical solutions. The dotted lines marked μ^c_{NL} in Figure 6 are eyeball estimates of the onset of NL zonation.

The onset of zonostrophic instability requires significantly smaller values of μ_* in the NL case than in the QL case: in Figure 6 the ratio $\mu^c_{\mathrm{QL}}/\mu^c_{\mathrm{NL}}$ is as large as five. Thus the QL system is much more unstable than the NL system. Regarding this quantitative difference between NL and QL, we recall that QL (and CE2) is an approximation based on dropping the eddy-eddy nonlinearity. This approximation is most defensible when the mean flow is very strong i.e., in cases where the zonal mean flow contains almost all of the energy. Therefore CE2 is not likely to be quantitatively accurate near the linear stability boundary, where the zonal mean flow is weak or nonexistent. The comparison in Figure 6 is thus a worst case test of CE2. How, or if, CE2 might be improved to account for the missing eddy-eddy nonlinearity in this weak mean-flow regime is an open issue.

Zonostrophically stable NL solutions

Figure 7 shows two NL solutions which are zonostrophically stable i.e., these solutions have

$$\mu^c_{\mathrm{NL}} < \mu_*\,, \tag{75}$$

and $\langle \mathrm{zmf} \rangle \approx 0$. In the left panel of Figure 7 the drag is so heavy that the approximate dominant balance in (1) is $\mu\zeta \approx \xi$ and the vorticity field closely resembles a snapshot of the forcing ξ.

Figure 8 compares energy spectra of statistically steady QL and NL solutions. With strong drag (i.e., $\mu_* = 0.309$) only the directly forced wavenumbers are significantly excited. As μ_* is reduced there is transfer of energy to small

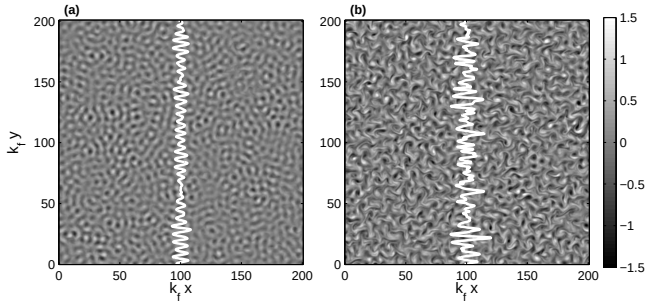

FIG. 7. Snapshots of the vorticity $\zeta(x,y,t)$ with overlaid zonally averaged vorticity $-U_y(y,t)$ (solid white curve) with (a) $\mu_* = 0.309$ and, (b) $\mu_* = 0.0545$. Both snapshots are at non-dimensional time $2\mu t = 25$, after spin-up from rest, and $\beta_* = 1$.

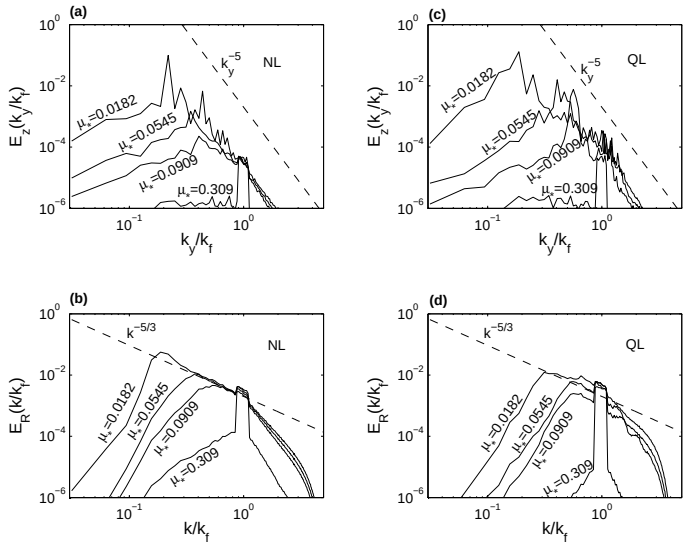

FIG. 8. The upper panels show the zonal spectrum, $E_{\rm Z}(k_y/k_f)$, for QL and NL solutions with $\beta_* = 1$. The lower panels show the residual spectrum $E_{\rm R}(k/k_f)$, defined as the angularly averaged spectrum after removal of the "zonal modes" with $k_x = 0$. The largest peak in $E_{\rm Z}(k_y/k_f)$ defines the wavenumber $m_{\rm Z}$, even if there are no quasi-steady steady zonal jets e.g., as in the NL simulation with $\mu_* = 0.0545$ in panel (a).

wavenumbers. In the NL case the transfer of energy to wavenumbers smaller than k_f is the due to the inverse energy cascade. In the QL case the excitation of small wavenumbers is due only to shearing by the zonal mean flow. Comparing QL and NL solutions at the same value of μ_*, one sees from Figures 8(b) and 8(d), that there is significantly more low-wavenumber eddy energy in the NL cases. Yet the zonal mean energy is always stronger in the QL case. There is no clear association between the inverse energy cascade and zonation.

The NL solution shown in right panel of Figure 7 with $\mu_* = 0.0545$ has an eddy energy spectrum in Figure 8 (b) exhibiting the beginning of $-5/3$ range. However this solution has $\langle \text{zmf} \rangle \approx 0$ and thus serves as example of an isotropic, spatially homogeneous, weakly turbulent, β-plane flow, without jets. To activate zonostrophic instability the drag μ_* must be reduced e.g., to $\mu_* = 0.0182$ in Figures 1 and 8.

The jet scale

If zonation occurs, as evinced by significantly nonzero values of $\langle \text{zmf} \rangle$, then by counting the number of distinct jets one can reliably estimate[3] a jet wavenumber $m_{\rm J}$. For example, in Figure 1 there are seven jets and therefore $m_{\rm J}/k_f = 7/32$.

However we noticed that there are cases without jets in which the zonal energy spectrum $E_{\rm Z}(k_y/k_f)$ has a strong peak: an example is the $\mu_* = 0.0545$ solution in Figure 7(b): the corresponding zonal energy spectrum in Figure 8(a) has a distinct peak even though there are no zonal jets. In cases like this, we report a wavenumber $m_{\rm Z}$ which is the peak of the zonal spectrum $E_{\rm Z}(k_y/k_f)$. In cases where there are strong jets we invariably find that $m_{\rm Z} \approx m_{\rm J}$. It is interesting to compare $m_{\rm J}$ and $m_{\rm Z}$ with a Rhines wavenumber defined as

$$m_{\rm Rh} = \sqrt{\frac{\beta}{2V_{\rm RMS}}}\,, \tag{76}$$

where the root mean square velocity is

$$V^2_{\rm RMS} \stackrel{\rm def}{=} \left\langle \frac{1}{(2\pi L)^2} \int U^2 + u'^2 + v'^2 \, {\rm d}a \right\rangle . \tag{77}$$

We investigated other choices for the velocity in the Rhines wavenumber e.g., Rhines (1975) advocated the RMS of v'. We found however that $V_{\rm RMS}$ gave the best estimate of the NL jet spacing at small values of μ_*. An advantage of $V_{\rm RMS}$ is that the energy power integral[4] can be used to express $V_{\rm RMS}$ in terms of external parameters as

$$\varepsilon \approx \mu V^2_{\rm RMS}\,. \tag{78}$$

The relation above applies with an error (due to hyperviscous dissipation) of less than 5% in our simulations. Sub-

[3] In certain cases the system may be transitioning between a state with n and $n+1$ jets. Following Panetta (1993), we then count $n+\frac{1}{2}$ jets; no other fractional values are permitted.

[4] From (1), the exact energy power integral is $\langle \psi\xi + \mu|\boldsymbol{\nabla}\psi|^2 + (-1)^{n-1}\nu_n|\boldsymbol{\nabla}^{n-1}\zeta|^2\rangle = 0$, where $\langle\rangle$ is both a domain integral and a time average.

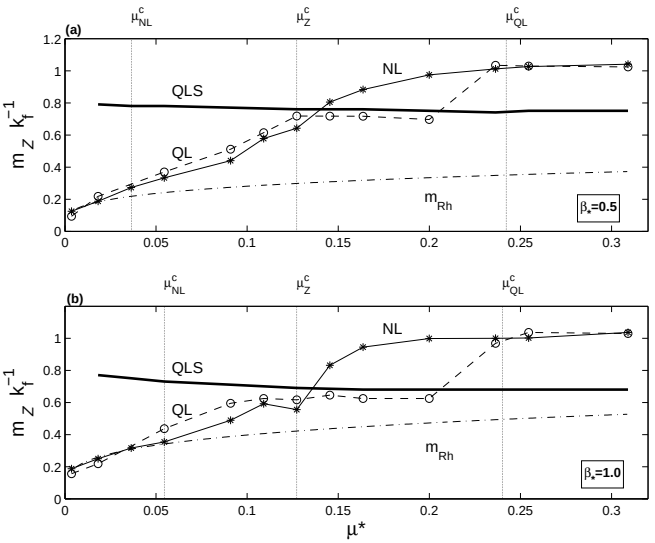

FIG. 9. A summary of zonal wavenumbers (jet scales) for solutions with (a) $\beta_* = 0.5$ and (b) $\beta_* = 1$. The dot-dashed curve is the Rhines wavenumber defined in (79). The solid curve labelled QLS is most unstable wavenumber calculated from the dispersion relation (47). The NL solutions are indicated by $*$ and the QL solutions by $\circ$.

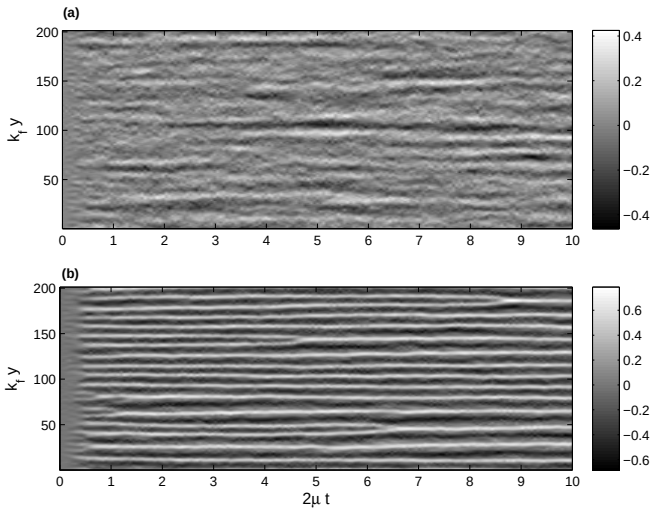

FIG. 10. Hovmöller diagrams for the (a) NL and (b) QL runs with β_*=1.0 and $\mu_* = 0.0545$. The NL run corresponds to the vorticity snapshot shown in Fig. 7(b) and shows zonal "streaks". In panel (b) the QL jets initially appear at a wavenumber predicted by linearization of CE2. Then successive mergers result in an increase in jet spacing.

stituting (78) into (76) one has

$$m_{\rm Rh} \approx k_f \left(\frac{\beta_* \mu_*^{1/2}}{2} \right)^{1/2} . \qquad (79)$$

Figure 9 compares the zonal wavenumber $m_{\rm Z}$ obtained from QL and NL solutions with the Rhines wavenumber on the right of (79), and with the most-unstable wavenumber obtained from the linear stability analysis of section 4. In Figure 9 we show only the $\beta_* = 1$ and $\beta_* = 0.5$ solutions: solutions with other values of β_* exhibit a broadly similar dependence of $m_{\rm Z}$ on μ_*.

At large values μ_* only the directly forced modes are excited, and consequently $m_{\rm Z} \approx k_f$ in both the QL and NL cases. At the critical value $\mu_* = \mu^c_{\rm QL}$ in Figure 9, the QL solutions undergo zonostrophic instability, and close to this transition, e.g., at $\mu_* = 0.2$ and 0.165 in Figure 9(a), the QL $m_{\rm Z}$ agrees with the analytic result from Figure 5. In this regime the NL solutions start to develop an inverse cascade (but without exciting zonal jets) and the NL $m_{\rm Z}$ begins to decrease.

There is an interesting transition at $\mu_* = \mu^c_Z$ in Figure 9. At this point the QL and NL zonal wavenumbers are equal, and as μ_* is reduced the QL and NL wavenumbers are locked together. At $\mu_* = \mu^c_{\rm NL}$ in Figure 9 the NL solutions finally become zonostrophically unstable, resulting in NL jets and significantly non-zero values of NL $\langle {\rm zmf} \rangle$. At the smallest value of μ_* in Figure 9, which corresponds to the runs in Figures 1 and 2, the QL and NL wavenumbers are almost equal, and are estimated roughly by $m_{\rm Rh}$.

In Figure 9 the analytic result QLS agrees with the observed QL jet scale only when μ_* is not too far from the linear stability boundary $\mu^c_{\rm QL}$. In the strongly unstable regime, with μ_* significantly less than $\mu^c_{\rm QL}$, the observed wavenumber $m_{\rm Z}$ is much smaller than the most unstable wavenumber predicted by linear theory. This increase in the QL jet scale is a result of merging jets which initially appear with a spacing which is well predicted by the linear theory. This phenomenology begins at about $\mu_* = \mu^c_Z$ and is illustrated in Figure 10.

Figure 10(a) shows the Hovmöller diagram of the jetless NL solution from Figure 7(b). There is no zonation and $U(y,t)$ shows "streaks" rather than jets. These streaks are not strong relative to the turbulent eddy field i.e., $\langle {\rm zmf} \rangle \approx 0$. The corresponding zonal energy spectrum in Figure 8(a) exhibits a strong peak, which is a signature of these transient zonal steaks.

Figure 10(b) shows the QL case in which jets initially appear with a relatively small meridional spacing predicted by linear theory, followed by a sequence of mergers so that the mature flow has $m_{\rm Z}$ much less than the most linearly unstable wavenumber. The QL jet-merging phenomenology, which is effectively a one-dimensional inverse cascade, is very similar to the "Cahn-Hilliard" solutions obtained by Manfroi and Young (1999) from a model of determinis-

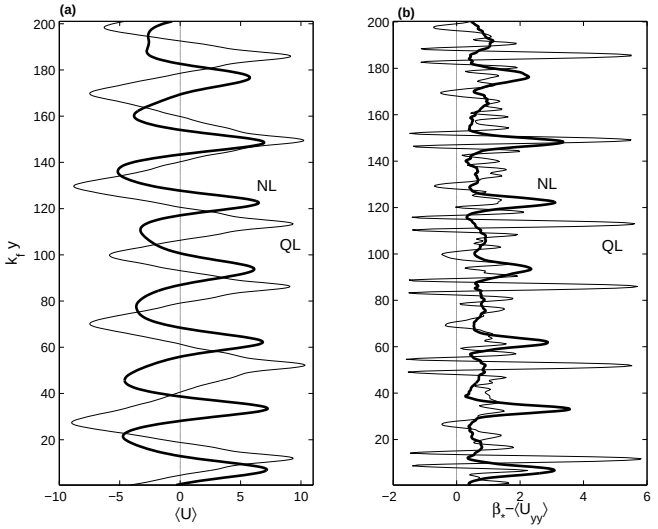

FIG. 11. Comparison of zonal mean velocity profiles of the $\beta_* = 1$ NL and QL runs in Figures 1 and 2.

tically forced zonation.

The small drag regime

The flows in Figure 1 and 2 have relatively light damping and both flows have organized jets containing a substantial fraction of the total kinetic energy. Figure 11 shows the time-averaged zonal mean-flow, $\langle U \rangle$ and the corresponding potential vorticity (PV) gradient, $\beta_* - \langle U_{yy} \rangle$. In Figure 2 the QL jets are almost symmetrical in the zonal direction, in contrast to the NL jets[5]. But the QL jets are not perfectly symmetric: the PV gradient in Figure 11(b) reveals the QL east-west asymmetry. The NL PV gradient is positive for all y and thus the NL jets are stable according to the Rayleigh-Kuo criterion. The QL PV gradient in Figure 11(b) reverses sign on the flanks of the eastward jet, and also at the centers of the westward jets. Nonetheless the QL zonal mean flow shows no indication of barotropic instability i.e., the deep spikes with $\beta_* - \langle U_{yy} \rangle < 0$ are permanent features of the QL zonal mean flow even after time averaging.

Via integration of their SSST system, Farrell and Ioannou (2007) report equilibrated zonal mean flows with much stronger east-west asymmetry than the QL flow in Figure 11 e.g., see their figures 8 and 9. There are at least[6] two non-dimensional parameters, β_* and μ_*, and the jet profile depends on both of these. We will not attempt to characterize this variation systematically. However to make some contact with the strong-forcing limit considered by Farrell and Ioannou (2007) we consider the QL solution in Figure 10(b) and in Figure 12(a), and increase the energy injection rate ε by a factor of one thousand, while holding β, μ and k_f approximately fixed. Then from (45), the control parameters β_* and μ_* are each reduced by a factor of ten. The time averaged zonal-mean profile of this strongly forced solution is shown in Figure 12(b), and exhibits the parabolic velocity profile seen in the NL run in Figure 1: there are fast eastward jets with sharp gradients and broad westward jets with smaller PV gradients. Also, the time averaged QL jet-profile in Figure 12(b) is more asymmetric than the weaker forced QL jet shown in Figure 12(a), that has a forcing that is a factor of 10 smaller. In order to quantify the jet asymmetry, we use the ratio

$$\alpha(\beta_*, \mu_*) = \frac{U_{\max}}{|U_{\min}|}\,, \tag{80}$$

where $U_{\max}$ and $U_{\min}$ are the maximum and mimimum values attained in the zonal-mean velocity profile. By increasing the forcing strength by a factor of 1000, the jet asymmetry increases from $\alpha = 1.25$ in Figure 12(a) to $\alpha = 1.56$ for the profile in Figure 12(b). This is smaller than the "ideal", marginally stable (i.e. $\beta - U_{yy} = 0$ everywhere except at the eastward jet where the PV jumps) profile considered in Danilov and Gurarie (2004), which has $\alpha = 2$.

Thus, although a detailed study of QL jet asymmetry is not a focus of the present work, our QL numerical solutions are thus generally consistent with the equilibrated SSST jets presented in Farrell and Ioannou (2007).

Discussion of the eddy-eddy nonlinearity

An important effect of eddy-eddy nonlinearity is the stirring of PV, producing an exponential-in-time reduction in the length scale of vorticity fluctuations. Eddy-driven stirring is removed from the QL system by (6): shearing by $U(y,t)$ is the only scale-reduction mechanism acting on the QL eddy vorticity. The small-scale structure evident in the QL PV gradient in the right panel of Figure 11 may reflect the relative inefficiency of shearing by $U(y,t)$ at removing vorticity fluctuations.

Further differences in the jet structure evident in Figure 11 can be explained by meandering of the NL jets, so that the zonal average reduces the sharpness of the NL PV gradient. The spectral signature of the NL jet meanders is a high energy mode at $(k_x, k_y) = (1/32, 6/32)k_f$ in the two-dimensional NL spectrum; this same mode is only weakly excited in the QL spectrum. The excitation of almost-zonal modes, with a small but non-zero of value of k_x, is a well known aspect of zonation. These are called a "satellite modes" by Danilov and Gurarie (2004), and

[5] If $\beta = 0$ then the equations of motion are invariant under $y \to -y$ and $\psi \to -\psi$. This symmetry, which induces $u \to u$, is broken in both QL and NL by non-zero β. This explains the characteristic east-west asymmetry of $U(y,t)$ on the β-plane

[6] Farrell and Ioannou (2007) also employ a forcing with a different correlation functon than our isotropic choice.

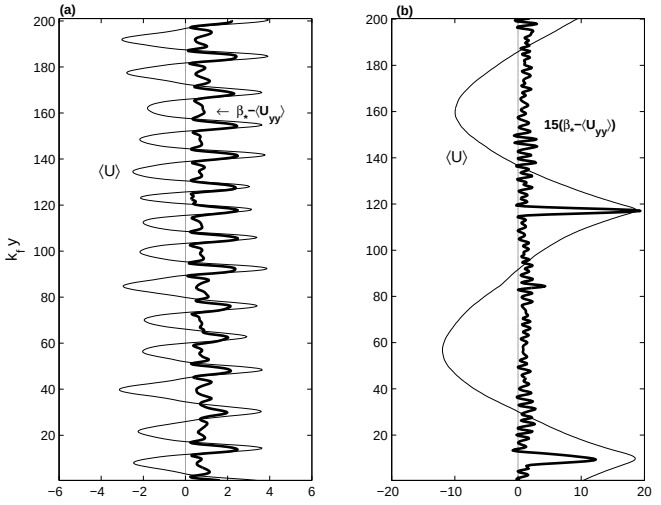

FIG. 12. Comparison of time-averaged zonal-mean velocity profiles (thin lines) of QL runs. Panel (a) is the solution from Figure 10(b) with $\beta_* = 1.0$ and μ_*=0.054 and panel (b) is the strongly forced solution with $\beta_* = 0.1$ and μ_*=0.005. Also plotted are the corresponding PV gradients (thick curves).

they correspond to a domain-scale meander of the NL jets, which is not present in the QL case.

7. Discussion and conclusion

A contribution of this work is the analytic development of the linearized theory of zonostrophic instability within the context of the second-order cumulant expansion (CE2) of Marston et al. (2008), and the stochastic structural stability theory (SSST) of Farrell and Ioannou (2003, 2007). These statistical formulations are equivalent to the correlation dynamics derived in section 3, and that physical-space formulation, in terms of partial differential equations for the correlation functions Ψ and $\mathcal{Z}$, provides some insight into the mathematical structure of CE2/SSST.

In the upper panel of Figure 5 we display the curve of neutral zonostrophic stability in the (β_*, μ_*)-parameter plane obtained by solution of linearized CE2 dynamics. We have shown that with isotropic forcing zonostrophic instability is not a negative-viscosity instability: the hallmark of a negative-viscosity instability is that at the stability boundary the most unstable wavenumber is zero. The deterministic model of anisotropically forced β-plane zonation analyzed by Manfroi and Young (1999) provides a bona fide example of the negative-viscosity case. Instead, for the isotropically and stochastically forced model analyzed here, the onset of zonostrophic instability is at the non-zero meridional wavenumber shown in the bottom panel of Figure 5; only at large β_* does this wavenumber approach zero. Moreover, in Section 5 we showed that with isotropic forcing the CE2 eddy viscosity ν_e is identically zero.

Comparison of QL and NL numerical solutions indicates that the CE2 linear stability boundary does not provide an accurate estimate of the onset of zonostrophic instability for NL flows. This quantitative failure of CE2 is not surprising: neglect of the eddy-eddy nonlinearity is most plausible in cases where most of the energy is in the zonal mean flow: close to the stability boundary the zonal-mean flow is only incipient. An outstanding open problem is improving CE2 to account for the missing physics in the eddy-eddy nonlinearity. Another important problem is obtaining analytic insight into the solution of the CE2 system in the regime where CE2 is likely to be valid i.e., in the strongly unstable regime where the drag μ_* is much less than the critical drag μ^c and the fraction of energy in the zonal-mean flow is substantial.

Acknowledgments.

This work was supported by the National Science Foundation under OCE1057838. We thank Nikos Bakas, Oliver Bühler, George Carnevale, Brian Farrell, Petros Ioannou, Brad Marston and Steve Tobias and for discussion of these results.

APPENDIX A

Implementation of the random forcing $\xi(\boldsymbol{x}, t)$

For numerical purposes we model the δ-correlated forcing $\xi(x, y, t)$ in (1) using a discrete approximation. The goal is to construct a statistically isotropic and narrow band forcing localized close to a radial wavenumber k_f. Thus the forcing is confined to an annulus $\mathcal{A}$ in wavenumber space, where wavenumbers $\boldsymbol{k}$ in $\mathcal{A}$ satisfy the inequality

$$k_f + \delta k < |\boldsymbol{k}| < k_f - \delta k\,. \tag{A1}$$

We take $\delta k = k_f/8$, so that $\mathcal{A}$ is tightly around the average radius k_f. We use a fourth-order Runge Kutta scheme, with time step δt. Implementing the Runge-Kutta scheme requires the value of the forcing not just at points in time separated by the time step δt but also at the mid-points. Some care must be exercised here though, since the Runge-Kutta scheme assumes a certain degree of smoothness of the solution. To ensure this, we use a forcing that during the n'th time step, when $(n-1)\delta t < t < n\delta t$, has the form

$$\xi(\boldsymbol{x}, t) = \sum_{\boldsymbol{k}_i \in \mathcal{A}} \{\xi_i(n-1) + [\xi_i(n) - \xi_i(n-1)]\chi_n(t)\}\, e^{i\boldsymbol{k}_i\cdot\boldsymbol{x}}\,, \tag{A2}$$

where $\chi_n(t) \stackrel{\text{def}}{=} (t/\delta t) - (n-1)$ varies linearly from zero to one during the n'th time step. The coefficient $\xi_i(n)$ above

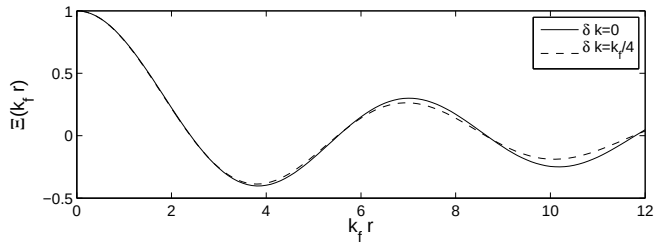

FIG. 13. Comparison of the ring forcing, $\delta k \to 0$ (solid line) and the narrow-band forcing with $\delta k = k_f/4$ (dashed line).

is

$$\xi_i(n) = \sqrt{\frac{2\varepsilon k_f^2}{N_{\mathcal{A}}\delta t}}\, \mathrm{e}^{\mathrm{i}\phi_i(n)}\,, \tag{A3}$$

where $N_{\mathcal{A}}$ is the number of wavevectors in $\mathcal{A}$, and $\varepsilon = -\langle\psi\xi\rangle$ is the rate of energy injection. The dependence $\xi_i(n) \propto 1/\sqrt{\delta t}$ ensures that the forcing is $\delta-$correlated in the limit $\delta t \to 0$. The phase, $\phi_i(n)$, is a random variable, chosen from a uniform distribution in $[0, 2\pi]$; the phase is set independently for each wavevector $\boldsymbol{k}_i$, and resets at the start of each time step.

The narrow-band forcing is described by the correlation function,

$$\tilde{\Xi}^b(k) = \frac{2\pi\varepsilon k_f}{\delta k}\begin{cases}1\,, & \text{if } k_f - \delta k < k < k_f + \delta k;\\ 0\,, & \text{otherwise,}\end{cases} \tag{A4}$$

which has the physical-space form

$$\begin{aligned}\Xi^b(r) &= \frac{\varepsilon k_f}{\delta k}\int_{k_f-\delta k}^{k_f+\delta k} J_0(kr)\, k\mathrm{d}k\,,\\ &= \frac{2\varepsilon k_f}{r^2\delta k}\left[zJ_1(z)\right]_{(k_f-\delta k)r}^{(k_f+\delta k)r}\,.\end{aligned} \tag{A5}$$

A comparison of $\Xi^b(r)$ and its idealized form, $\Xi(r) \propto J_0(k_f r)$ is shown in Figure 13

APPENDIX B

Rapid temporal decorrelation: derivation of (20)

The crucial assumption leading to (20) is that the temporal de-correlation of the forcing is rapid, as indicated by the $\delta(t_1-t_2)$ on the right of (10). Operationally, this means that we might integrate (8) during the first time step from $t = 0$ to $t = \delta t$ as

$$\zeta'(\boldsymbol{x},\tau) = \zeta'(\boldsymbol{x},0) + \sqrt{\delta t}\times\hat{\xi}(\boldsymbol{x}) + \delta t\times \mathrm{AOT}(\boldsymbol{x},0)\,, \tag{B1}$$

where $\mathrm{AOT}(\boldsymbol{x},0)$ indicates "all other terms" in (8), evaluated at $t = 0$. Also in (B1), $\hat{\xi}(\boldsymbol{x})$ is a spatial random field with correlation function

$$\Xi(x, y_1, y_2,) = \overline{\hat{\xi}(\boldsymbol{x}_1)\hat{\xi}(\boldsymbol{x}_2)}\,. \tag{B2}$$

The forcing $\hat{\xi}$ "renovates" during each time step i.e., in the n'th time step one creates a new independent realization of $\hat{\xi}$, but always with the same spatial correlation function Ξ. According to this recipe the magnitude of $\hat{\xi}$ is independent of δt as $\delta t \to 0$, and therefore $\xi = \hat{\xi}/\sqrt{\delta t} \to \infty$ as $\delta t \to 0$. As demanded by this argument, notice that $\xi_i(n)$ in (A3) is proportional to $1/\sqrt{\delta t}$.

Before ensemble averaging, we can multiply (B1) evaluated at $\boldsymbol{x}_1$ with (B1) evaluated at $\boldsymbol{x}_2$ to obtain

$$\begin{aligned}\zeta_1'(\delta t)\zeta_2'(\delta t) = \zeta_1'(0)\zeta_2'(0) &+ \sqrt{\delta t}\left[\zeta_1'(0)\hat{\xi}_2 + \zeta_2'(0)\hat{\xi}_1\right]\\ &+ \delta t\left[\hat{\xi}_1\hat{\xi}_2 + \zeta_1'(0)\mathrm{AOT}_2(0) + \zeta_2'(0)\mathrm{AOT}_1(0)\right]\\ &+ O\left(\delta t^{3/2}\right)\,,\end{aligned} \tag{B3}$$

where the subscript n indicates evaluation at $\boldsymbol{x}_n$ e.g.,

$$\zeta'(\boldsymbol{x}_1,\delta t) = \zeta_1'(\delta t)\,. \tag{B4}$$

Upon ensemble averaging, the terms of order $\sqrt{\delta t}$ on the right of (B3) vanish because $\hat{\xi}(\boldsymbol{x})$ is independent of $\zeta'(\boldsymbol{x},0)$. Thus

$$\begin{aligned}\frac{\mathcal{Z}(\delta t)-\mathcal{Z}(0)}{\delta t} =& \Xi + \overline{\zeta_1'(0)\mathrm{AOT}_2(0)} + \overline{\zeta_2'(0)\mathrm{AOT}_1(0)}\\ &+ O\left(\delta t^1\right)\,.\end{aligned} \tag{B5}$$

As $\delta t \to 0$ the left hand side is the time derivative of the vorticity correlation function. The $\sqrt{\delta t}$-terms in (B3), which prohibit a differentiable limit, are nulled in (B5) by the ensemble average. Thus, taking the limit $\delta t \to 0$ in (B5), we obtain the deterministic differential equation (18) for the evolution of the correlation function $\mathcal{Z} \equiv \overline{\zeta_1\zeta_2}$.

APPENDIX C

Derivation of the dispersion relation (41)

The linearized equations resulting from substitution of (40) into (29) and (26) are

$$\begin{aligned}\left(s + 2\mu + \tfrac{1}{2}\nu m^2 - 2\nu\nabla^2\right)\hat{\mathcal{Z}} + 2i\sin\left(\frac{my}{2}\right)\Phi_{\mathsf{H}x}\hat{U}(m)&\\ - 2im\beta\hat{\Psi}_{xy} = 0\,,&\end{aligned} \tag{C1}$$

$$\left(s + \mu + \nu m^2\right)\hat{U}(m) + im\hat{\Psi}_{xy}\big|_{x=y=0} = 0\,, \tag{C2}$$

$$\left(\nabla^2 + im\partial_y - \tfrac{1}{4}m^2\right)\left(\nabla^2 - im\partial_y - \tfrac{1}{4}m^2\right)\hat{\Psi} = \hat{\mathcal{Z}}\,, \tag{C3}$$

where in (C1)

$$\Phi_{\mathsf{H}} \stackrel{\text{def}}{=} \mathcal{Z}_{\mathsf{H}} + m^2\nabla^2\Psi_{\mathsf{H}} = \left(\nabla^4 + m^2\nabla^2\right)\Psi_{\mathsf{H}}\,. \tag{C4}$$

A key intermediate step on the path to (C1) is noting $U_1 = U\left(\bar{y} + \frac{1}{2}y\right)$ and $U_2 = U\left(\bar{y} - \frac{1}{2}y\right)$, so that with $U(y,t)$ in (40) one has

$$U_1 - U_2 = 2i\sin\left(\frac{my}{2}\right)\mathrm{e}^{im\bar{y}+st}\,\hat{U}(m) + c.c.\,. \tag{C5}$$

Applying the Fourier transform in (33) to (C1) and (C3), one has

$$\left[2im\beta pq + h_+^2 h_-^2 s'\right]\tilde{\Psi} + ip\hat{U}\left(\tilde{\Phi}_{\mathsf{H}}^- - \tilde{\Phi}_{\mathsf{H}}^+\right) = 0\,, \tag{C6}$$

$$\frac{im}{\bar{s}}\iint pq\,\tilde{\Psi}\,\frac{\mathrm{d}p\,\mathrm{d}q}{(2\pi)^2} = \hat{U}\,, \tag{C7}$$

$$h_+^2 h_-^2\tilde{\Psi} = \tilde{\mathcal{Z}}\,. \tag{C8}$$

In (C6) through (C8) we use the notation

$$h_\pm \stackrel{\text{def}}{=} \sqrt{p^2 + (q \pm m/2)^2}\,, \tag{C9}$$

$$\tilde{\Phi}_{\mathsf{H}}^\pm \stackrel{\text{def}}{=} h_\pm^2\left(h_\pm^2 - m^2\right)\tilde{\Psi}_{\mathsf{H}}(p, q \pm m/2)\,, \tag{C10}$$

$$\bar{s} \stackrel{\text{def}}{=} s + \mu + \nu m^2\,, \tag{C11}$$

$$s' \stackrel{\text{def}}{=} s + 2\mu + \tfrac{1}{2}\nu m^2 + 2\nu h^2\,. \tag{C12}$$

Eliminating $\hat{U}(m)$ between (C6) and (C7), we obtain the dispersion relation

$$\bar{s} = m\Lambda_-\left(s', m\right) - m\Lambda_+\left(s', m\right)\,, \tag{C13}$$

where the functions $\Lambda_+(s', m)$ and $\Lambda_-(s', m)$ are defined by the integral

$$\Lambda_\pm(s', m) \stackrel{\text{def}}{=} \iint p^2 q\,\frac{h_\pm^2\left(h_\pm^2 - m^2\right)\tilde{\Psi}_{\mathsf{H}}(p, q \pm m/2)}{s'\,h_+^2 h_-^2 + 2im\beta pq}\,\frac{\mathrm{d}p\,\mathrm{d}q}{(2\pi)^2}\,. \tag{C14}$$

Changing variables with $p \to -p$ and $q \to -q$, and using the exchange symmetry in (17), one finds that

$$\Lambda_-(s', m) = -\Lambda_+(s', m)\,, \tag{C15}$$

so that the right of (C13) is equal to $2m\Lambda_-$. Then with the change of variables $q' = q - m/2$ in the Λ_- integral, and using (37), one can write the dispersion relation (C13) as

$$\bar{s} = \iint \frac{p^2\left(h_{++}^2 - h^2\right)h^2\left(h^2 - m^2\right)}{s'\,h^2 h_{++}^2 + i\beta p\left(h_{++}^2 - h^2\right)}\,\frac{\tilde{A}(p,q)}{2\mu + 2\nu h^2}\,\frac{\mathrm{d}p\,\mathrm{d}q}{(2\pi)^2}\,, \tag{C16}$$

where $h_{++} \stackrel{\text{def}}{=} \sqrt{p^2 + (q+m)^2}$.

If the forcing is isotropic then $\tilde{A}(p,q) = \tilde{A}\left(h\right)$, and the integral on the right of (C16) can be simplified using polar coordinates $(p,q) = h(\cos\theta, \sin\theta)$:

$$\beta^2\bar{s} = \int_0^\infty h^4\left(h^2 - m^2\right)\frac{\tilde{A}(h)}{2\mu + 2\nu h^2}\,S\left(\frac{s'h^2}{\beta m}, \frac{m}{h}\right)\,\frac{\mathrm{d}h}{2\pi}\,, \tag{C17}$$

where S is the function

$$S(\chi, n) \stackrel{\text{def}}{=} \oint \frac{\cos^2\theta\,(2\sin\theta + n)}{\chi\left(1 + 2n\sin\theta + n^2\right) + \mathrm{i}\cos\theta\,(2\sin\theta + n)}\,\frac{\mathrm{d}\theta}{2\pi}\,. \tag{C18}$$

One can show that $S(\chi, n) = -S(-\chi, n) = -S(\chi, -n)$, and therefore $S(0, n) = S(\chi, 0) = 0$. These symmetries are important for further work, and they are not manifest from the definition of S in (C18). Thus we seek an alternative form with more obvious properties. The change of variables $\theta \to \theta + \pi$ results in

$$S(\chi, n) = \oint \frac{\cos^2\theta\,(-2\sin\theta + n)}{\chi\left(1 - 2n\sin\theta + n^2\right) - \mathrm{i}\cos\theta\,(-2\sin\theta + n)}\,\frac{\mathrm{d}\theta}{2\pi}\,. \tag{C19}$$

The average of (C18) and (C19) is then

$$S(\chi, n) = \chi n \times \underbrace{\oint \frac{\cos^2\theta\,(1 + n^2 - 4\sin^2\theta)}{\left[\chi + \mathrm{i}\sin 2\theta\right]^2 + n^2\left[\chi^2(n^2 + 2 - 4\sin^2\theta) + \cos^2\theta\right]}\,\frac{\mathrm{d}\theta}{2\pi}}_{\stackrel{\text{def}}{=} Q(\chi, n)}\,. \tag{C20}$$

The function $Q(\chi, n)$ is manifestly an even function of n, and $\theta \to -\theta$ shows that Q is also an even function of χ.

Substituting (C20) into (C17) gives the dispersion relation in the form

$$\beta^2\bar{s} = \int_0^\infty h^5\left(h^2 - m^2\right)\frac{\tilde{A}(h)\,s'}{2\mu + 2\nu h^2}\,Q\left(\frac{s'h^2}{\beta m}, \frac{m}{h}\right)\,\frac{\mathrm{d}h}{2\pi}\,. \tag{C21}$$

With $\nu = 0$, we obtain the dispersion relation in (41).

APPENDIX D

The function $Q(\chi, n)$

In this appendix we summarize some properties of the function $Q(\chi, n)$ defined in (C20). We first note that

$$\begin{aligned} Q(\chi, 0) &= \int_0^{2\pi}\frac{\cos^2\theta\,(1 - 4\sin^2\theta)}{(\chi + i\sin 2\theta)^2}\,\frac{\mathrm{d}\theta}{2\pi}\,, \\ &= 1 - \frac{|\chi|(2\chi^2 + 3)}{2\left(\chi^2 + 1\right)^{3/2}}\,. \end{aligned} \tag{D1}$$

If $0 \le n^2 \le 1$ then

$$\begin{aligned} Q(0, n) &= 1 + \mathrm{Pr}\int_0^{2\pi}\frac{1}{n^2 - 4\sin^2\theta}\,\frac{\mathrm{d}\theta}{2\pi}\,, \\ &= 1\,, \end{aligned} \tag{D2}$$

where 'Pr' refers to the Cauchy-principal value.

The case $\beta_* \ll 1$ requires the approximation of $Q(\chi, n)$ in the limit $\chi \to \infty$. One can expand the integrand in

inverse powers of χ and integrate term by term. The first two non-zero terms are

$$Q(\chi,n) = \frac{3}{2^3\chi^4(1-n^2)} + \frac{5}{2^5\chi^6}\frac{(n^4+2n^2-4)}{(1-n^2)^3} + O\left(\chi^{-8}\right). \quad \text{(D3)}$$

The case $\beta_* \gg 1$ requires the approximation of $Q(\chi,n)$ in the limit $\chi \to 0$. A somewhat laborious 'range-splitting' calculation shows that

$$Q(\chi,n) = 1 - \frac{3}{2}\frac{24-7n^2}{24-6n^2}|\chi| + O\left(\chi^2\right). \quad \text{(D4)}$$

Finally, if $\chi \to \infty$, with $n = 0$ then from either (D1) or (D3) we obtain

$$Q(\chi,0) = \frac{3}{8\chi^4} + O\left(\chi^{-6}\right). \quad \text{(D5)}$$

APPENDIX E

The neutral curve

The neutral curve in the (β_*, μ_*)-parameter plane is defined by the conditions in (49). For the dispersion relation in (47), these take the form,

$$\mu\beta^2 = 2(1-m^2)Q\left(\chi_0, m\right), \quad \text{(E1)}$$

$$m = \frac{(1-m^2)^2}{\mu\beta^2}\frac{\partial Q\left(\chi_0,m\right)}{\partial m}, \quad \text{(E2)}$$

with $\chi_0 = 2\mu/m\beta$ above. (For brevity, in this Appendix, we drop the $*$'s indicating non-dimensional variables.) An examination of the numerical values of χ_0 on the neutral curve motivates the possibility that $\chi_0 \to \infty$ as $\beta \to 0$ and $\chi_0 \to 0$ as $\beta \to \infty$. We now use this numerical observation to derive analytical approximations for the neutral curve in the complementary limiting cases $\beta \to 0$ and $\beta \to \infty$. To this end, we use the approximations to $Q(\chi,m)$ summarized in Appendix D.

Approximation of the marginal curve, $\beta \gg 1$ and $\chi_0 \ll 1$

First in the case of $\beta \to \infty$, we have from (D4)

$$Q(\chi_0,m) = 1 - \frac{\mu}{\beta}\left(\frac{3}{m} + \frac{5m}{8}\right) + O(m^2\chi_0). \quad \text{(E3)}$$

Clearly, neglecting the $O(m\chi_0)$ term must be justified *post-facto* once a consistent dominant balance is found. Substituting (E3) in the neutral curve equations, (E1) and (E2) and keeping in mind that that $\beta^{-1} \ll 1$, we get

$$\frac{\mu\beta^2}{2} = (1-m^2) - \frac{3\mu}{m\beta} + \frac{29\mu m}{8\beta} + O\left(\mu m^2\beta^{-1}\right), \quad \text{(E4)}$$

$$m^3 = 3\beta^{-3} + O\left(m^2\beta^{-3}\right). \quad \text{(E5)}$$

The only consistent balance in the m-equation corresponds to $m^3 \sim 3\beta^{-3}$ and consequently,

$$m = \frac{3^{1/3}}{\beta} + O(\beta^{-3}). \quad \text{(E6)}$$

Since $m \sim O(\beta^{-1})$ the only consistent balance in (E1) is $\mu \sim 2\beta^{-2}$. A higher order estimate for μ can be derived by substituting for m to get

$$\mu = \frac{2}{\beta^2}\left(1 - \frac{3^{5/3}}{\beta^2}\right) + O(\beta^{-6}). \quad \text{(E7)}$$

These approximate expressions are superimposed on the numerically obtained neutral curve in the Fig. 5 with agreement once $\beta > 2$.

Approximation of the marginal curve, $\beta \ll 1$ and $\chi_0 \gg 1$

A similar analysis is used when $\beta \to 0$ for which, we can write from (D3),

$$Q(\chi_0,m) = \frac{3}{2^7}\left(\frac{\beta}{\mu}\right)^4\left(\frac{m^4}{1-m^2}\right) + \frac{5}{2^{11}}\left(\frac{\beta}{\mu}\right)^6\left[\frac{m^6(m^4+2m^2-4)}{(1-m^2)^3}\right] + O(\chi_0^{-8}), \quad \text{(E8)}$$

$$\quad \text{(E9)}$$

and therefore

$$\partial_m Q(\chi_0,m) = \frac{3}{2^6}\left(\frac{\beta}{\mu}\right)^4\left[\frac{m^3(2-m^2)}{(1-m^2)^2}\right] - \frac{5}{2^{11}}\left(\frac{\beta}{\mu}\right)^6\left[\frac{m^5(4m^6-6m^4-16m^2+24)}{(1-m^2)^4}\right] + O(\chi_0^{-9}). \quad \text{(E10)}$$

Substituting into equations (E1) and (E2) one has

$$\mu\beta^2 = \frac{3}{2^6}\left(\frac{\beta}{\mu}\right)^4 m^4 + \frac{5}{2^{10}}\left(\frac{\beta}{\mu}\right)^6\left[\frac{m^7(m^4+2m^2-4)}{(1-m^2)^2}\right] + h.o.t., \quad \text{(E11)}$$

$$m = \frac{3}{2^6}\frac{\beta^2}{\mu^5}m^2(2-m^2) - \frac{5}{2^{11}}\frac{\beta^4}{\mu^7}\left[\frac{m^5(4m^6-6m^4-16m^2+24)}{(1-m^2)^2}\right] + h.o.t. \quad \text{(E12)}$$

Above, *h.o.t.* refers to the higher order terms that have been neglected from the above equation and can be justified to be small *post-facto*. In (E11), assuming a dominant balance between the term on the left and the first term on the right, we have

$$\mu \sim \left(\frac{3}{64}\right)^{1/5}\beta^{2/5}m^{4/5}. \quad \text{(E13)}$$

Similarly from (E12)

$$m \sim \frac{3}{2^6}\frac{\beta^2}{\mu^5} m^3(2-m^2)\,, \tag{E14}$$

which on substituting for μ from (E13), gives us $m \sim 1$ and

$$\mu \sim \left(\frac{3}{64}\right)^{1/5} \beta^{2/5}\,. \tag{E15}$$

Proceeding to the next order, we obtain after some algebra

$$m \approx 1 - \underbrace{\frac{5^{1/3}}{3^{7/15}2^{19/15}}}_{\approx 0.43}\, \beta^{2/5}\,. \tag{E16}$$

As in the case before, we plot this estimate for m against the numerical estimate in Figure 5 and the agreement is excellent. In fact the approximations to $m^{\rm c}(\beta)$ practically span the entire range of the neutral curve.

The small-m expansion

When $m \to 0$ with all other parameters fixed, we observe in Figure 4 that $s \to -\mu$ and therefore in (47) the first argument of Q is

$$\frac{s+2\mu}{m\beta} \approx \frac{\mu}{m\beta} \gg 1\,. \tag{E17}$$

To compute the small-m expansion of the dispersion relation we write $s = -\mu + s_1$ and use (D5) to approximate Q. Thus the dispersion relation (47) becomes

$$\beta^2 s_1 \approx \frac{3}{8}\,\frac{m^4\beta^4}{\mu^4}\,. \tag{E18}$$

This produces the small-m version of the dispersion relation in (55).

REFERENCES

Bakas, N. A. and P. Ioannou, 2011a: On the mechanism underlying the spontaneous generation of barotropic zonal jets. *submitted to J. Atmos. Sci.*, ???

Bakas, N. A. and P. Ioannou, 2011b: Structural stability theory of two-dimensional fluid flow under stochastic forcing. *in press J. Fluid Mech.*, ???

Carnevale, G. F. and P. C. Martin, 1982: Field theoretical techniques in statistical fluid dynamics: with applications to nonlinear wave dynamics. *Geophys. Astrophys. Fluid Dynamics*, **20**, 131–164.

Cox, S. M. and P. C. Matthews, 2005: Exponential time differencing for stiff systems. *J. Comp. Phys.*, **176**, 430–455.

Cummins, P. F. and G. Holloway, 2010: Reynolds stress and eddy viscosity in direct numerical simulation of sheared-two-dimensional turbulence. *J. Fluid Mech.*, **657**, 394–412.

Danilov, S. and V. M. Gryanik, 2004: Barotropic beta-plane turbulence in a regime with strong zonal jets revisited. *J. Atmos. Sci.*, **61**, 2283–2295.

Danilov, S. and D. Gurarie, 2004: Scaling, spectra and zonal jets in beta-plane turbulence. *Physics of Fluids*, **16**, 2592–2603.

DelSole, T., 2001: A theory for the forcing and dissipation in stochastic turbulence models. *J. Atmos. Sci.*, **58**, 3762–3775.

Diamond, P. H., S.-I. Itoh, K. Itoh, and T. S. Hahm, 2005: Zonal flows in plasmas — a review. *Plasma Physics and Controlled Fusion.*, **47**, R35–R161.

Farrell, B. F. and P. J. Ioannou, 1993a: Stochastic forcing of perturbation variance in unbounded shear and deformation flows. *J. Atmos. Sci.*, **50**, 200–211.

Farrell, B. F. and P. J. Ioannou, 1993b: Stochastic forcing of the linearized navier-stokes equations. *Phys. Fluids A*, **5**, 2600–2609.

Farrell, B. F. and P. J. Ioannou, 2003: Structural stability of turbulent jets. *J. Atmos. Sci.*, **50**, 2101–2118.

Farrell, B. F. and P. J. Ioannou, 2007: Structure and spacing of jets in barotropic turbulence. *J. Atmos. Sci.*, **64**, 3652–3665.

Galperin, B., S. Sukoriansky, N. Dikovskaya, P. Read, Y. Yamazaki, and R. Wordsworth, 2006: Anisotropic turbulence and zonal jets in rotating flows with a β-effect. *Nonlinear Processes in Geophysics*, **13**, 1–16.

Holloway, G., 2010: Eddy stress and shear in 2d flows. *J. Turbulence*, **11**, 1–14.

Huang, H. P. and W. A. Robinson, 1998: Two-dimensional turbulence and persistent zonal jets in a global barotropic model. *Nonlinear Processes in Geophysics*, **55**, 611–632.

Lilly, D. K., 1969: Numerical simulation of two-dimensional turbulence. *Physics of Fluids*, **I2(supplement)**, II240–II249.

Maltrud, M. E. and G. K. Vallis, 1991: Energy spectra and coherent structures in forced two-dimensional and beta-plane turbulence. *J. Fluid Mech.*, **228**, 321–342.

Manfroi, A. J. and W. Young, 1999: Slow evolution of zonal jets on the beta-plane. *J. Atmos. Sci.*, **56**, 784–800.

Marston, J. B., E. Conover, and T. Schneider, 2008: Statistics of an unstable barotropic jet from a cumulant expansion. *J. Atmos. Sci.*, **65**, 1955–1966.

Nozawa, T. and S. Yoden, 1997: Formation of zonal-band structure in forced two-dimensional turbulence on a rotating sphere. *Physics of Fluids*, **9**, 2081–2093.

O'Gorman, P. A. and T. Schneider, 2007: Recovery of atmospheric flow statistics in a general circulation model without nonlinear eddy-eddy interactions. *Geophys. Res. Lett.*, **34 (L22801)**.

Panetta, L., 1993: Zonal jets in wide baroclinically unstable regions: persistence and scale selection. *J. Atmos. Sci.*, **50**, 2073–2106.

Rhines, P. B., 1975: Waves and turbulence on a beta-plane. *J. Fluid Mech.*, **69**, 417–443.

Salmon, R., 1998: *Lectures on Geophysical Fluid Dynamics*. Oxford University Press, xiii+379 pp.

Scott, R. K. and L. M. Polvani, 2007: Forced-dissipative shallow-water turbulence on the sphere and the atmospheric circulation of the giant planets. *J. Atmos. Sci.*, **64**, 3158–3176.

Shepherd, T. G., 1985: Time development of small disturbances to plane couette flow. *J. Atmos. Sci.*, **42**, 1868–1871.

Tobias, S. M., K. Dagon, and J. Marston, 2011: Astrophysical fluid dynamics via direct statistical simulation. *Astrophysical J.*, **727**, 1–12.

Vallis, G. K. and M. E. Maltrud, 1993: Generation of mean flow and jets on a beta plane and over topography. *J. Phys. Oceanogr.*, **23**, 1346–1362.

Vasada, A. R. and A. P. Showman, 2005: Jovian atmospheric dynamics: an update after *galileo* and *cassini*. *Reports on Progress in Physics*, **68**, 1935–1996.

Williams, G. P., 1978: Planetary circulations: 1. barotropic representation of jovian and terrestrial turbulence. *J. Atmos. Sci.*, **35**, 1399–1426.